American Mineralogist, Volume 63, pages 641–663, 1978

Phase compositions through crystallization intervals in basalt–andesite–H_2O at 30 kbar with implications for subduction zone magmas

CHARLES R. STERN

Lamont-Doherty Geological Observatory of Columbia University
Palisades, New York 10964

AND PETER J. WYLLIE

Department of Geophysical Sciences, University of Chicago
Chicago, Illinois 60637

Abstract

The melting relationships of a gabbro (olivine tholeiite, quartz eclogite composition) and tonalite (andesite composition) with varying amounts of H_2O added were determined at 30 kbar pressure using piston–cylinder apparatus. With 5 percent H_2O, clinopyroxene and garnet are the liquidus minerals for the basalt, and they occur together throughout the crystallization interval from 1260° to 760°C. With 5 percent H_2O, garnet is the liquidus phase for andesite at 1200°C and it crystallizes alone through 100°C; garnet and clinopyroxene occur together through the rest of the crystallization interval from 1100° to 740°C. Compositions of garnets, clinopyroxenes, and glasses were measured with electron microprobe at the following temperatures: tonalite, 1175° (Ga,Gl), 1100° (Ga,Cpx,Gl), 1000° (Ga,Cpx,Gl), 900° (Cpx,Gl); gabbro, 1200° (Ga,Cpx), 1100°C (Ga,Cpx). Published data by T. H. Green and Ringwood on hydrous and anhydrous calc–alkaline rock compositions, combined with these new data, define compositional trends for minerals through the upper parts of crystallization intervals. From these trends and thermodynamic constraints for mineral pairs, the compositions of minerals through the complete crystallization intervals were calculated. Using calculated mineral compositions and estimated mineral proportions, the compositions of equilibrium liquid paths were calculated through the crystallization intervals of hydrous and anhydrous basalts, basaltic andesite, and andesite. Compositions of quenched liquids in the crystallization interval of andesite with 5 percent H_2O measured with the electron microprobe agree well with calculated compositions, supporting the validity of the calculated liquid paths. Equilibrium liquid paths for basalts and andesites at 30 kbar diverge from the average chemical variation trend of typical calc–alkaline rocks (basalt–andesite–dacite–rhyolite). With decreasing temperature and increasing SiO_2 content, the liquid paths increase in Ca/(Mg+Fe) compared with the average trend, more so for hydrous compositions than for anhydrous. With equilibrium partial fusion of quartz eclogite, the first liquids are richer in SiO_2 than average andesites, significantly so if H_2O is present. Liquids with SiO_2 content corresponding to andesites occupy no distinctive position such as a thermal valley; they are situated within a continuous sequence of liquid compositions. Partial melting of subducted ocean crust at 100 km depth produces liquids with a range of intermediate SiO_2 contents, but these must be modified by fractionation at shallower depths if they are to reach the surface with chemistry corresponding to average calc–alkaline lavas.

Introduction

Recent andesites and associated calc–alkaline rocks occur above Benioff zones of seismic activity, which mark the position at depth of subducted oceanic crust and lithosphere. The reported petrochemical variations of igneous rocks transverse to volcanic arcs have suggested to many geologists that there is a correlation between the chemistry of erupted rocks and the depth to the seismic zone (Kuno, 1966, 1968; Dickinson, 1968, 1973; Dickinson and Hatherton, 1967; Sugimura, 1968; Jakeš and White, 1970; Lopez-

0003–004X/78/0708–0641$02.00

Escobar *et al.*, 1977). If there is such a correlation, the chemical variations reported should be explicable in terms of the phase relationships of the materials involved, provided that the processes are known. Unfortunately, the processes have not been adequately defined, nor have the phase relationships of possible materials yet been determined in sufficient detail for critical tests to be made of competing hypotheses.

The simplest proposal is that primary intermediate and acid calc–alkaline magmas form by different degrees of partial melting of oceanic crust, consisting mostly of abyssal olivine tholeiite (partly metasomatized and metamorphosed) and siliceous sediments, which descended into the mantle in a subduction zone (Stille, 1955; Coats, 1962; Green and Ringwood, 1968; Ringwood, 1969; Armstrong, 1968; Hamilton, 1969a, 1969b; Dickinson, 1970; Oxburgh and Turcotte, 1970; Marsh and Carmichael, 1974). The fusion is presumed to occur at depths between 75 and 350 km, the depth to active Benioff zones beneath calc–alkaline volcanoes (Dickinson, 1971, 1973), in the presence of small proportions of water carried in hydrous minerals (Raleigh and Lee, 1969; Jakeš and White, 1970). Melting may occur in amphibole eclogite or quartz eclogite, with or without free H_2O (Green and Ringwood, 1968; Boettcher, 1973; Wyllie, 1973; Ringwood, 1975, chapter 7; Allen *et al.*, 1975). More complex proposals involve magmas generated within the overlying mantle peridotite, associated with influx of H_2O or siliceous melts from the subducted ocean crust (Kushiro, 1973; Boettcher, 1973; Nicholls and Ringwood, 1973).

Whatever the source and conditions of generation of magmas, they may be subjected to fractionation at various levels. The minerals involved in fractional crystallization include combinations of garnet, clinopyroxene, amphibole, and plagioclase, with each combination producing different effects in terms of major and trace elements. The chemistry of volcanic rocks suggests that the processes involved are complex rather than simple (Ringwood, 1975, chapter 7; Kay, 1977).

For evaluation of the proposed processes, we must know the phase relationships of the observed magmatic products, the calc–alkaline plutonic and volcanic rock series, and of the inferred source materials, mantle peridotite and oceanic crust, including sediments, through the pressure range extending from the surface to the deep sources. Knowledge of the compositions of phases through the melting intervals is essential.

Experimental approach

In a pioneering study, Green and Ringwood (1968) determined the phase relationships of anhydrous olivine tholeiite, quartz tholeiite, basaltic andesite, and andesite compositions at 18, 27, and 36 kbar. They measured the compositions of garnets and clinopyroxenes in near-liquidus runs, and estimated their proportions. From these data they calculated equilibrium paths of liquids for up to 35 percent crystallization. They concluded that, in the range 27–36 kbar, fractional crystallization of basalt, as well as "liquid fractionates" from quartz eclogite bulk composition, broadly follow the calc–alkaline trend, and that the low-melting composition is andesitic. Experiments with uncontrolled H_2O contents indicated that the low-melting fraction under hydrous conditions is more siliceous. This was confirmed by experiments on andesite and rhyodacite compositions with 2 percent, 5 percent, and 10 percent H_2O (Green and Ringwood, 1972; Green, 1972).

We are concerned here with processes at 30 kbar, involving garnet and clinopyroxene. Amphiboles of subducted oceanic crust are already dehydrated at this pressure (Lambert and Wyllie, 1968, 1972; Wyllie, 1973), so we offer no additional review of experiments related to amphibole, nor of the controversies concerning the effect of H_2O on peridotite.

In 1971, when Stern began to study the melting relationships of oceanic sediments for evaluation of their role in subduction zones, it became evident that the results should be considered with respect to phase relationships of basalt–andesite–rhyolite–H_2O (Stern, 1973). This led to extension of a general research program on the effect of H_2O on the rock series gabbro–tonalite–granodiorite–granite as a function of P–T–X_{SiO_2}–X_{H_2O} (Wyllie, 1977). Stern *et al.* (1975) summarized the phase relationships to 35 kbar of gabbro, tonalite, and granite with excess H_2O, and the H_2O-undersaturated liquidus surfaces. Stern and Wyllie (1973) outlined phase relationships at 30 kbar for gabbro–tonalite–granite with variable H_2O contents, and compared the results with those for a pelagic red clay. Experimental details concerning iron loss to capsules and the problem of attaining reversible equilibrium have been published (Stern and Wyllie, 1975).

In this paper, we present Stern's (1973, 1974) experimental results on two rocks with varying amounts of H_2O at 30 kbar. The rocks are a gabbro (quartz eclogite, olivine tholeiite composition) modeling subducted ocean crust and erupted basalt, and a

tonalite modeling erupted andesite. Phases in selected runs with 5 percent H_2O were analyzed with the electron microprobe.

We have combined the new data for garnet and clinopyroxene with the published data, and extended the results of Green and Ringwood (1968) and Green (1972) through the crystallization intervals. For lower temperatures, where small crystals and close intergrowths prevent satisfactory microprobe measurements, mineral compositions were calculated by extrapolating the compositional trends and imposing thermodynamic conditions for mineral pairs. Liquid compositions through the crystallization intervals for basalt, basaltic andesite, and andesite, dry and with H_2O, were calculated from mineral compositions and modes (measured or estimated). Glass compositions for andesite with 5 percent H_2O measured by electron microprobe agree closely with the calculated liquid compositions, indicating that the calculation procedure provides good values for successive liquid compositions, with some reservations discussed below. We conclude that the equilibrium liquid paths diverge somewhat further from the average andesite–rhyodacite compositions than suggested by Green and Ringwood (1968) and Green (1972).

Table 1. Chemical analyses, CIPW norms, and approximate modes of rocks studied

	Gabbro DW-1	Tonalite 101
Chemical Analyses		
SiO_2	45.91	59.14
TiO_2	0.94	0.79
Al_2O_3	17.19	18.23
Fe_2O_3	2.33	2.32
FeO	7.67	3.62
MnO	0.22	0.11
MgO	7.48	2.50
CaO	13.54	5.92
Na_2O	1.63	3.81
K_2O	0.14	2.19
H_2O^+	1.78	0.82
H_2O^-	1.26	0.04
P_2O_5	0.04	0.30
CO_2	-	0.01
Total	100.13	99.80
CIPW Norms		
Qz	-	11.7
Or	0.83	12.9
Ab	13.78	32.2
An	39.14	26.2
Di	22.59	0.9
Hy	6.95	9.4
Ol	8.55	-
Mt	3.39	3.4
Il	0.78	1.5
Ap	0.10	0.7
Modes		
Quartz	-	1.3
Alkali feldspar	-	4.5
Plagioclase	47	59
Augite	47	-
Biotite	-	12.5
Hornblende	-	9
Olivine	3(serp.)	-
Opaque minerals	3	2

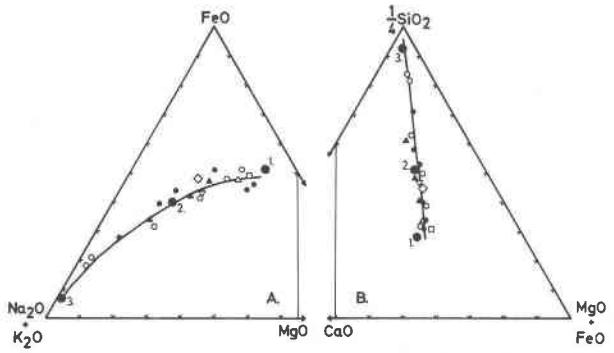

Fig. 1. Chemical compositions of calc–alkaline rocks (total Fe calculated as FeO). Compositions plotted are: this study, large solid circles (1, gabbro DW-1; 2, tonalite 101; 3, granite 104; see Table 1, and Stern and Wyllie, 1973); other experimental starting compositions (small solid circles from Green and Ringwood, 1968; solid triangles from Green, 1972); typical compositions of the Taupo volcanic zone, New Zealand (empty circles, Carmichael *et al.*, 1974); representative and average compositions (square, average high-alumina basalt from Kuno, 1960, Table 6; upright triangle, average central type basalt from Nockolds, 1954, p. 1021; upside-down triangle, average calc–alkaline andesite from Taylor and White, 1966; diamond, average Cenozoic andesite, from Chayes, 1969). The line through these points is taken as the average chemical variation trend of calc–alkaline rocks.

Rock starting materials

The compositions, CIPW norms, and modes of the rocks used are given in Table 1. The gabbro is a fine-grained, high-alumina olivine tholeiite from a sill in Soay, Scotland (Wyllie and Drever, 1963; Table 5, analysis 5). It has low SiO_2 and high CaO compared to an average oceanic tholeiite (Engel *et al.*, 1965); and low SiO_2, Na_2O and K_2O, and high CaO and MgO compared to typical high-alumina basalts.

The tonalite, from the Central Sierra Nevada Batholith of California, is specimen 101 of Piwinskii (1968a). Piwinskii (1968b) compiled details of its mineralogy, petrology, and field accounts. The tonalite has composition similar to andesites from Mount Hood (Wise, 1969) and Fiji (Green, 1972), as well as average andesites (Taylor and White, 1966) and other andesite compositions used in experimental studies (Green and Ringwood, 1968), as shown in Figure 1.

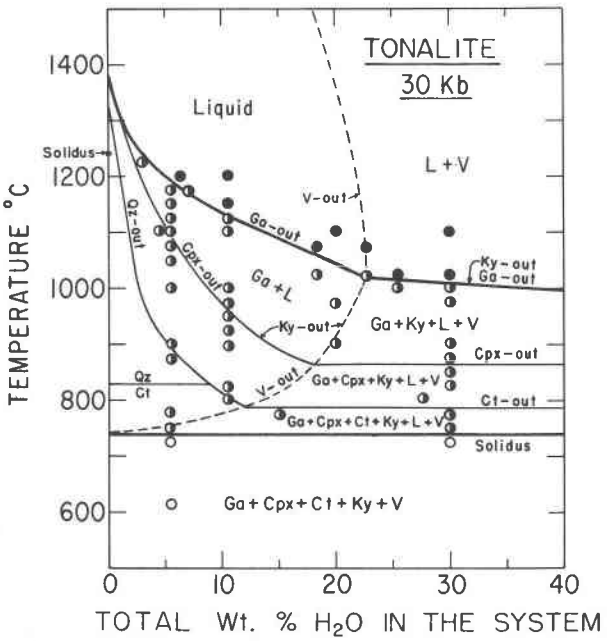

Fig. 2. Isobaric melting relations of tonalite (andesite composition, Table 1) with varying H_2O contents. The position of the vapor-out curve is uncertain. Abbreviations: Ga–garnet, Cpx–clinopyroxene, Qz–quartz, Ct–coesite, Ky–kyanite, L–liquid, V–vapor.

The chemistry of andesites and other calc–alkaline and associated rocks has been the subject of many reviews (see Carmichael *et al.*, 1974, chapter 11; Wyllie, 1971, chapter 7). Although the precise chemical relationships among the volcanic and plutonic rocks of volcanic island arcs and continental margins remain uncertain, the line in Figure 1A defines what is conventionally accepted as the average chemical variation of calc–alkaline rocks (Carmichael *et al.*, 1974, Figure 12-2). The points plotted include typical volcanic rocks, and compositions that have been used in previous experimental studies (Green and Ringwood, 1968). The familiar AFM plot is supplemented by Figure 1B, which shows in addition the variation in SiO_2 and CaO/(MgO+FeO).

Our experiments have been conducted with three rocks which plot as the large circles 1, 2, and 3 in Figure 1. These rocks, a gabbro, a tonalite, and a granite, represent one composition join through the rock system. Here we are concerned initially with rocks 1 and 2, but the near-coincidence of the composition join (Fig. 4) with the average chemical variation (Fig. 1) is used later (see Figs. 14 and 15).

Experimental methods

The powdered rock samples (passed through 200-mesh) were sealed, with measured amounts of distilled and deionized water, within platinum and silver–palladium ($Ag_{30}Pd_{70}$, $Ag_{75}Pd_{25}$) alloy capsules, and reacted in single-stage piston–cylinder apparatus (Boyd and England, 1960), using a half-inch diameter tungsten carbide pressure chamber with hardened steel liner. All runs were brought to final pressure by the hot piston-out procedure (Boyd *et al.*, 1967); pressure was raised 5 to 7 kbar above run pressure, the sample was heated to run temperature, and the pressure was released to the run value. No friction correction was applied to the nominal pressure, which is considered accurate to ±5 percent.

Temperature was measured with chromel–alumel ($T \leq 850°C$) or Pt/Pt 10Rh ($T > 850°C$) thermocouples, with no correction applied for pressure effects on output emf. Temperatures are precise to ±5°C and probably accurate to within ±13°C at 1000°C, 30 kbar pressure, considering pressure effects on thermocouple emf (Getting and Kennedy, 1971).

Electron microprobe analysis of selected runs was performed on a 4-spectrometer ARL-EMX microprobe. Standards and samples were carbon-coated together to avoid discrepancies in coat thickness. Samples were analyzed for eight elements: Si, Ti, Al, Fe, Mg, Ca, Na, and K. The standards used were a diopside with 2 percent Ti for Mg and Ti; an anorthite, An_{100}, for Si and Ca; an augite pyroxene for Fe; an albite for Na; and a sanidine for K. An acceleration voltage of 15 kV, a sample current of 0.2 microamps, and counting times of 10 seconds were used for all analyses. Between 5 and 10 point analyses were made on both standards and sample phases. For runs with more than 70 percent glass, an automatic scanning beam was used for analyzing glass in order to minimize volatilization of alkalis. For other runs, the areas of glass were too small for the scanning beam. Some samples were etched for ten seconds with concentrated fluoroboric acid. This created a slight relief between glass and crystalline phases without changing the relative major-element concentrations by more than 2 percent (2 to 10 percent for Na) (Anderson, 1974). Raw data were examined for inconsistencies, corrected for instrumental factors (background, detector dead-time, beam-current drift) using a program written by I. Steele, and for matrix effects (absorption, fluorescence, and atomic number effect) using a program written at the Geophysical Laboratory (Boyd *et al.*, 1968; Hadidiacos *et al.*, 1970). The accuracy of the microprobe analysis is ±2 percent relative for each element of greater than 5 percent concentration, and ±5 percent for elements of less than 5

percent concentration. The detectability level is 0.5 percent.

Platinum and silver–palladium alloys absorb iron from silicate samples at high temperature (Yoder and Tilley, 1962; Muan, 1963). Merrill and Wyllie (1973) and Stern and Wyllie (1975) reviewed the problem for experiments similar to those conducted in this study. Green (1976) discussed ways to minimize or surmount this and other problems in rock–H_2O experiments. For our run times and temperatures, iron loss affects liquid compositions but not mineral compositions. Liquid compositions have been corrected for iron loss using time- and temperature-dependent correction factors determined by Stern and Wyllie (1975). According to Merrill and Wyllie (1975), the oxygen fugacity imposed on the reactants by the furnace assembly was slightly below the Ni/NiO buffer.

Table 2. Experimental runs analyzed with the electron microprobe

Run No.	Pres. Kb	Temp. °C	Water Added Wt. %	Time hr.	Capsule	Phases Present*
				Tonalite 101		
361	30	1000	25	1	$Ag_{30}Pd_{70}$	*Ga, L,* V
419	30	1100	18	1	$Ag_{75}Pd_{25}$	*L*
420	30	1100	18	3	$Ag_{75}Pd_{25}$	*L*
363	30	1100	15	1	$Ag_{30}Pd_{70}$	*L*
358	30	1100	15	1	Pt	*L*
357	30	1100	15	3	Pt	*L*
351	30	1100	15	3	$Ag_{30}Pd_{70}$	*L*
354	30	1100	15	10	$Ag_{30}Pd_{70}$	*L*
355	30	1100	15	10	Pt	*L*
308	30	900	10	2	$Ag_{30}Pd_{70}$	Ga, *Cpx,* Ky, L
307	30	950	10	1	$Ag_{30}Pd_{70}$	Ga, *L*
343	30	1000	10	2	$Ag_{30}Pd_{70}$	*Ga, L*
306	30	1125	10	1	$Ag_{30}Pd_{70}$	Ga, *L*
329	30	900	5	6	$Ag_{30}Pd_{70}$	Ga, *Cpx,* Ky, *L*
314	30	1000	5	3	$Ag_{30}Pd_{70}$	*Ga, Cpx,* Ky, *L*
316	30	1000	5	10	$Ag_{30}Pd_{70}$	*Ga, Cpx,* Ky, *L*
318	30	1100	5	1	$Ag_{30}Pd_{70}$	*Ga, L*
346	30	1100	5	1	Pt	Ga, *L*
344	30	1100	5	3	$Ag_{30}Pd_{70}$	*Ga,* Cpx, L
353	30	1100	5	10	$Ag_{30}Pd_{70}$	*Ga,* Cpx, L
310	30	1175	5	1	$Ag_{30}Pd_{70}$	*Ga, L*
416	30	1175	5	1	$Ag_{75}Pd_{25}$	*Ga,* L
405	30	1200	5	1	$Ag_{75}Pd_{25}$	*L*
356	30	1200	5	1	Pt	*L*
362	30	1200	5	3	Pt	*L*
406	30	1200	5	5	$Ag_{75}Pd_{25}$	*L*
408	30	1100	4	1	$Ag_{75}Pd_{25}$	*Ga, Cpx,* Ky, *L*
409	30	1100	4	5	$Ag_{75}Pd_{25}$	*Ga, Cpx, Ky, L*
				Gabbro DW-1		
414	30	1100	10	1	$Ag_{75}Pd_{25}$	*Ga,* Cpx, L
412	30	1100	5	1	$Ag_{75}Pd_{25}$	*Ga, Cpx,* L
411	30	1200	5	1	$Ag_{75}Pd_{25}$	*Ga, Cpx,* L

*L = Liquid; V = Vapor; Ga = Garnet; Cpx = Clinopyroxene; Ky = Kyanite; *X* = Phase X analyzed.

Phase relationships

Stern (1973) determined rock–H_2O diagrams at 30 kbar for the gabbro, tonalite, and granite plotted in Figure 1 as points 1, 2, and 3. Preliminary results were combined and discussed by Stern and Wyllie (1973). Details of the problem of iron loss to capsules, of run durations, and of establishing reversibility of phase boundaries within narrow temperature intervals were reviewed by Stern and Wyllie (1975). We present here results for the gabbro and tonalite, and the liquidus relationships for the series basalt–andesite–rhyolite–H_2O at 30 kbar. These provide the framework for location and discussion of the analyzed phases.

Andesite–H_2O

Figure 2 shows phase relationships for the tonalite composition with varying H_2O contents at 30 kbar. Details for selected runs are listed in Table 2. Experiments by Green (1972) and Green and Ringwood (1968) gave garnet as the liquidus phase for one anhydrous andesite, and clinopyroxene for another. The phase boundaries are extrapolated to the anhydrous rock composition from results of these two studies. The main difference between this diagram and an earlier version (Stern and Wyllie, 1973, Fig. 1) is delineation of the field for kyanite along the boundaries marked.

With increasing H_2O content, the phase boundary for clinopyroxene-out is depressed to progressively lower temperatures than that for garnet-out. The solubility of H_2O in tonalite (andesite) liquid at 30 kbar is 22.5 ± 2.5 weight percent, as given by intersection of the vapor-saturation boundary (dashed) with the liquidus.

Basalt–H_2O

Figure 3 shows phase relationships for the gabbro composition with varying H_2O contents at 30 kbar. Details for three runs are listed in Table 2; other details were reviewed by Stern and Wyllie (1975). The garnet-out and clinopyroxene-out boundaries could not be distinguished from each other for any H_2O content, and they are drawn coincident. Green and Ringwood (1968) gave clinopyroxene as the primary phase for anhydrous olivine basalt at 27 kbar, with garnet appearing 10°C below the liquidus. At 36 kbar garnet and clinopyroxene occurred together on the liquidus. Considering the results for basalt and andesite, we consider it likely that clinopyroxene is the liquidus phase, joined by garnet within a few degrees. The field for kyanite does not extend to the liquidus as it does in Figure 2. The runs are consistent with a

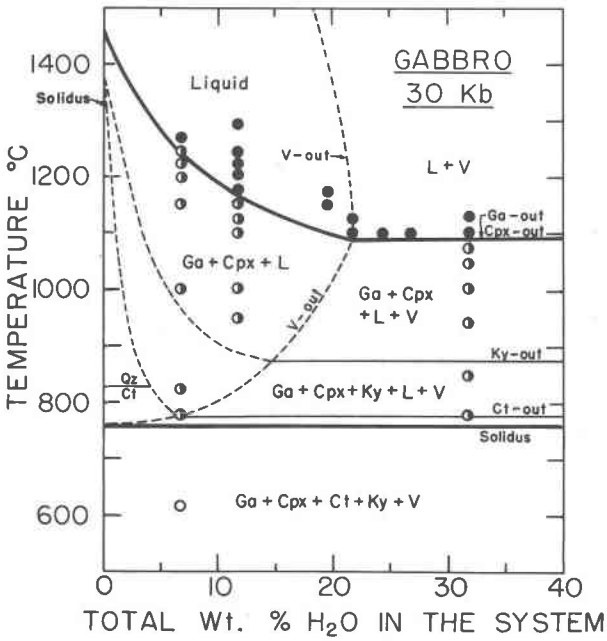

Fig. 3. Isobaric melting relations of gabbro (quartz eclogite, olivine tholeiite composition, Table 1) with varying H_2O contents. Note the uncertainty of the dashed phase boundaries for low H_2O contents; the vapor-out boundary may be steeper at low temperatures (compare Wyllie, 1971, p. 202), which would have the effect of increasing the temperature dependence of the vapor-absent phase boundaries. Abbreviations, see Fig. 2.

vapor-saturation boundary corresponding to H_2O solubility about the same as for the andesite.

Basalt–andesite–rhyolite–H_2O

Figure 4 shows selected phase relationships for the composition join basalt–andesite–rhyolite with varying amounts of H_2O at 30 kbar, constructed as described by Stern and Wyllie (1973). The liquidus for the dry series is based on the results of Green and Ringwood (1968) and Green (1972). They reported the thermal valley on the liquidus profile for andesitic compositions. We interpret this valley in terms of piercing points separating the fields for primary crystallization of quartz, garnet, and clinopyroxene. The clinopyroxene field is labeled "Cpx + Ga" because garnet appears so close to the liquidus temperature that the distinction is not readily made experimentally. The liquidus surface, contoured by lines of constant H_2O content from dry to H_2O excess, is based on Figures 2 and 3 and a similar diagram for granite–H_2O (Stern, 1973). Stern and Wyllie (1973, Fig. 2) illustrated the phase fields intersected by this composition join with 5 percent H_2O. The liquidus profile corresponds to the 5 percent H_2O contour in Figure 4, and the phase assemblages for the basalt and andesite compositions can be read from Figures 3 and 2, respectively.

The boundaries *mm'* and *cc'* divide the liquidus surface into three fields for the primary crystallization of quartz, of garnet, and of clinopyroxene (and garnet). With increasing H_2O content, the liquidus field for primary garnet, narrow near the dry liquidus, expands considerably at the expense of both quartz and clinopyroxene.

Measured phase compositions

Table 2 lists the runs that were analyzed. The compositions of garnets, clinopyroxenes, and quenched liquids (glasses) are listed in Tables 3, 4, and 5, respectively. Tonalite runs at some temperatures were repeated for comparison of the effects of different capsule materials, and of different run durations (see also Stern and Wyllie, 1975).

Garnets

For each run, at least ten individual garnet grains were analyzed. Reconnaissance indicated that garnets

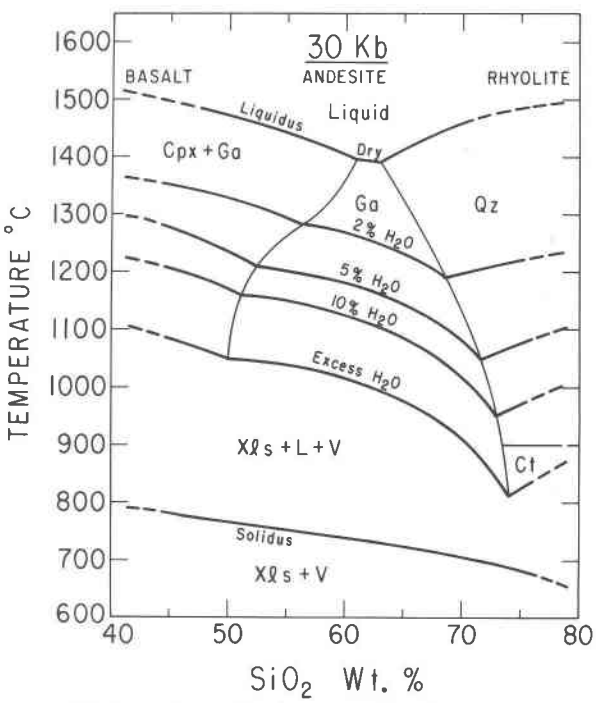

Fig. 4. Phase diagram for the composition join basalt–andesite–rhyolite, which corresponds closely with the average chemical variation line for calc–alkaline igneous rocks (Fig. 1). The isobaric liquidus surface for water contents varying from 0 percent to excess, and the crystallization interval with excess H_2O. Dry data from Green and Ringwood (1968), with H_2O from Stern and Wyllie (1973). For cross sections see Figs. 2 and 3 (59.14 percent SiO_2 and 45.91 percent SiO_2, respectively, Table 1). The solidus is independent of H_2O content. Abbreviations, see Fig. 2.

Table 3. Compositions, determined by microprobe analysis, of garnets in the melting intervals of tonalite and gabbro at 30 kbar

Composition	Tonalite 101											Gabbro DW-1		
Run #	310	416	408	409	318	344	353	314	316	343	361	411	412	414
Temp. °C	1175	1175	1100	1100	1100	1100	1100	1000	1000	1000	1000	1200	1100	1100
%H_2O	5	5	4	4	5	5	5	5	5	10	25	5	5	10
Capsule*	1	2	2	2	1	1	1	1	1	1	1	2	2	2
Time hr.	1	1	1	5	1	3	10	3	10	2	1	1	1	1
Co-existing Phases**			*Cpx* Ky	*Cpx* Ky		*Cpx*	Cpx	*Cpx* Ky	*Cpx* Ky			*Cpx*	*Cpx*	Cpx
SiO_2	40.2	40.2	39.5	39.1	40.3	40.3	40.2	38.6	39.0	39.2	39.7	40.4	40.2	40.4
TiO_2	0.7	0.8	1.4	1.2	1.0	1.0	1.0	2.4	1.4	1.5	1.5	0.3	0.6	0.3
Al_2O_3	22.5	22.4	22.3	22.4	21.4	22.5	21.7	21.6	21.5	21.1	21.6	22.9	22.6	23.0
FeO	16.3	15.6	18.9	18.7	17.6	18.2	19.1	21.6	22.7	19.6	17.7	12.3	15.6	13.9
MgO	11.6	10.8	8.6	8.6	9.7	8.7	9.7	8.3	7.0	7.9	9.8	13.0	11.1	12.0
CaO	10.9	8.8	9.9	10.2	11.6	11.3	9.8	9.6	11.6	11.1	12.8	10.4	11.2	11.0
Na_2O	0.1	0.1	0.2	0.2	0.1	0.1	0.2	0.2	0.2	0.2	0.1	0.0	0.0	0.0
Total	102.4	98.9	101.1	100.7	102.1	102.5	102.0	102.5	103.6	100.9	103.4	99.6	101.6	100.9
Structural Formulae on the Basis of 12 Oxygens***														
Si	2.94	3.01	2.96	2.94	2.90	2.97	2.98	2.89	2.91	2.96	2.91	2.97	2.95	2.96
Al^{IV} } $\Sigma Z \geq 3$	.05	.00	.04	.05	.01	.02	.01	.10	.08	.03	.08	.02	.04	.03
Al^{VI}	1.88	1.98	1.93	1.93	1.84	1.93	1.88	1.80	1.82	1.85	1.79	1.96	1.92	1.95
Ti } $\Sigma Y \geq 2$	.03	.04	.07	.07	.06	.06	.06	.13	.08	.09	.08	.02	.03	.01
Fe^{3+}	.07	.00	.00	.00	.09	.00	.05	.05	.09	.05	.12	.01	.04	.02
Fe^{2+}	.92	.97	1.18	1.17	.99	1.12	1.13	1.29	1.32	1.18	.96	.74	.91	.83
Mg } $\Sigma X \approx 3$	1.26	1.20	.96	.96	1.07	.95	1.07	.92	.77	.89	1.07	1.43	1.22	1.31
Ca	.85	.71	.80	.82	.92	.89	.78	.77	.92	.90	1.01	.82	.88	.86
x =	3.03	2.89	2.94	2.96	2.99	2.97	2.99	2.99	3.02	2.98	3.05	3.00	3.02	3.01
Mol. Prop.†														
Grossular	27.5	24.6	27.1	27.7	29.8	30.0	25.7	25.4	30.6	29.8	31.8	27.4	28.8	28.5
Pyrope	40.5	41.6	32.7	32.6	34.9	32.2	35.3	30.3	24.9	29.4	33.8	47.5	39.9	43.4
Almandine	32.0	33.8	40.2	39.7	35.3	37.8	39.0	44.3	44.5	40.8	34.4	25.1	31.3	28.1

*(1) $Ag_{30}Pd_{70}$, (2) $Ag_{75}Pd_{25}$.

**Liquid co-exists with all garnets. Compositions of phases in italics have been determined.

***$Al^{IV} = 3-Si$; $Al^{VI} = Al-Al^{IV}$; $Fe^{3+} = 2-(Al^{VI}+Ti)$; $Fe^{2+} = Fe-Fe^{3+}$.

†Calculated with $Fe^{2+} = \Sigma Fe$.

are homogeneous, within experimental limits imposed by the small size of the grains. Little change was noted from grain to grain in a single run. All garnet showed a small Na_2O content which is not due to contamination from surrounding or included glass, since such contamination would be accompanied by a detectable K_2O content. Garnet analyses with K_2O greater than 0.1 percent were considered contaminated and discarded. Total Fe in the garnets is calculated as FeO. In the structural formula of the analyzed garnets (Table 3) enough Fe^{3+} was assigned to the Y position to make Y = 2, but no consistent ratio of Fe^{3+}/Fe^{2+} was apparent. No correction was applied for iron loss, because tests confirmed that garnet compositions remain constant with changes in run duration (Stern and Wyllie, 1975). The trends of garnet compositions are considered in terms of the components almandine–pyrope–grossular, ignoring the TiO_2, Na_2O, and possible Fe_2O_3 contents of the garnets.

Figure 5 shows the trends of near-liquidus garnets (within 25°C of the liquidus) in andesite, as determined by Green (1972). Figure 5A shows the effect of pressure. With increasing pressure and constant H_2O content, the near-liquidus garnets show slight increase in Ca/(Ca + Mg) and decrease in Fe/Mg. Our new results at 30 kbar (Table 3) and Huang's unpublished result at 15 kbar are consistent. Results for dry andesite are parallel to those for andesite with 5 percent H_2O. The effect of increasing H_2O content at

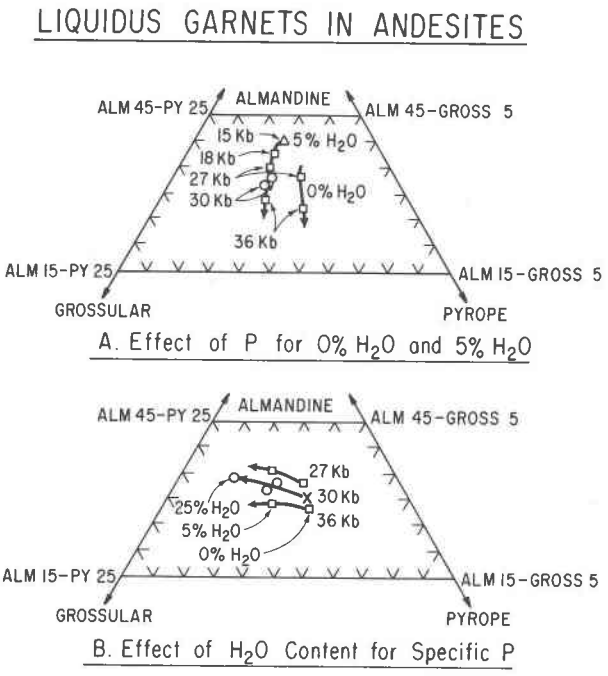

Fig. 5. The compositions of near-liquidus garnets in andesite. Circles at 30 kbar are listed in Table 3; the triangle at 15 kbar is from Huang (unpublished); squares at 18, 27, and 36 kbar are from Green (1972). (A) Trends with increasing pressure at constant H_2O contents; (B) trends with increasing H_2O contents at constant pressures. The point x is for garnet in anhydrous liquid at 30 kbar, as estimated by the intersection of the 0% H_2O trend in (A) with the 30 kb trend in (B).

a given pressure is shown in Figure 5B. Our new results at 30 kbar are consistent with those of Green (1972) at 27 and 36 kbar. With increasing H_2O content at constant pressure, Ca/(Mg + Fe) increases significantly. The concomitant slight increase in Fe/Mg is due to the decreasing liquidus temperature caused by increasing H_2O content, as shown in Figures 2 and 4.

Figure 6A shows the compositions of garnets through the crystallization intervals of andesite with 5 percent and 10 percent H_2O. The phase fields intersected as a function of temperature at 30 kbar are shown in Figure 2. Results of Green (1972) for 27 kbar show parallel trends for andesites with 5 percent and 10 percent H_2O, with slight separation for the effect of H_2O as indicated by Figure 5B. Our new data at 30 kbar with 5 percent H_2O show the same trend, with slight separation from the 27 kbar–5 percent H_2O trend for the effect of pressure as indicated by Figure 5A. With decreasing temperature, Fe/Mg increases significantly, and Ca/(Mg + Fe) increases very slightly.

Figure 6B shows that the garnet composition trends through the crystallization intervals of basaltic compositions with H_2O are similar to those for andesite–H_2O (Fig. 6A). The results of Green and Ringwood (1968) show little difference between the trends for garnets crystallizing from olivine tholeiite or quartz tholeiite at 27 kbar, although, for similar temperatures, Fe/Mg in garnet from quartz tholeiite is greater than that in olivine tholeiite. Our new data at 30 kbar with 5 percent and 10 percent H_2O for olivine tholeiite demonstrate the large increase in Ca/(Mg + Fe) caused by addition of H_2O to dry liquids (compare Fig. 5), and the much smaller change produced by increasing H_2O content from 5 percent to 10 percent (see Figs. 5B and 6A). The phase fields intersected at 30 kbar are shown in Figure 3.

Clinopyroxenes

At least ten separate clinopyroxene grains were analyzed for each experimental run. Some large

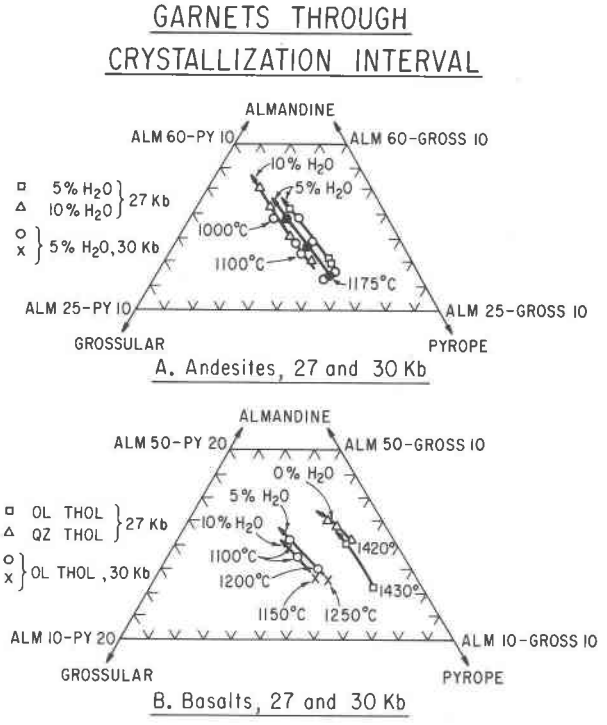

Fig. 6. Garnet compositions through the crystallization intervals of andesite and basalt at 27 and 30 kbar. (A) Trends for andesite with 5 percent and 10 percent H_2O at 27 kbar (Green, 1972), and with 5 percent H_2O at 30 kbar (Table 3); solid circles represent averages for open-circle runs made at the same temperature conditions. (B) Trends for anhydrous olivine basalt (squares) and quartz tholeiite (triangles) at 27 kbar (Green and Ringwood, 1968). Circles are for garnets from olivine tholeiite with 5 percent and 10 percent H_2O. Points x for olivine tholeiite at 30 kbar are plotted at the intersection of the garnet trends with the estimated trend of liquidus garnets with increasing H_2O content, based on the andesite lines in Fig. 5B.

grains varied in composition internally, but smaller grains appeared to be homogeneous, and these were used for analyses. Variation in Na_2O content between grains was minor compared with the variations between runs made at different conditions. Clinopyroxene analyses with more than 0.1 percent K_2O were discarded. No correction was made for the effects of iron loss. The analyzed clinopyroxenes in the melting interval of tonalite used to establish compositional trends occurred at 1000°C or lower, where the effects of iron loss are not great (Stern and Wyllie, 1975). Correcting the clinopyroxene composition for iron loss in the melting interval of the gabbro would not alter the conclusions reached in this study, as discussed below.

Extensive development of quench clinopyroxene near the liquidus of the gabbro made microprobe analysis of near-liquidus clinopyroxene uncertain. Clinopyroxene in run 411 at 1200°C (Table 4) is considered to be a quench pyroxene, or a mixture of quench and primary crystals. It has high FeO compared to the clinopyroxene in run 412 at 1100°C. At 1100°C, quench clinopyroxene was less of a problem.

Structural formulae of pyroxenes have been converted to molecular proportions by calculating all Na as jadeite, total Al minus the amount used in jadeite (equal to Na) as $\frac{1}{2}Al_2O_3$, and total Ca, Mg, and Fe as $\frac{1}{2}$wollastonite, $\frac{1}{2}$enstatite, and $\frac{1}{2}$ferrosilite. The TiO_2 content was neglected, in order to simplify calculations.

The trends of clinopyroxene compositions are illustrated in terms of components enstatite–wollastonite–ferrosilite, with supplementary diagrams for jadeite and Al_2O_3 proportions (Figs. 7 and 9). Some jadeite and Al_2O_3 data were omitted for clarity.

Figure 7 illustrates the trends reported by Green and Ringwood (1968) for clinopyroxenes through the crystallization interval of anhydrous quartz tholeiite at pressures of 18 kbar, 27 kbar, and 36 kbar. Fe/Mg, Ca/(Mg + Fe), jadeite, and Al_2O_3 all increase with decreasing temperature for all pressures. Trends are similar for the less complete data for other anhydrous compositions (except for the jadeite content for basaltic andesite, Fig. 7B). Figure 7A shows that with increasing pressure for anhydrous liquids, the clinopyroxene trend line is shifted towards higher Mg/Fe. The same shift is evident for trends at constant pressure for anhydrous liquids with lower SiO_2 contents.

New data for andesite with 5 percent H_2O at 30 kbar (Table 4) show a parallel trend in Figure 7A, but with considerable enrichment of the clinopyroxenes in Fe/Mg, which could be due in part to the lower temperatures of crystallization (see Figs. 2 and 4).

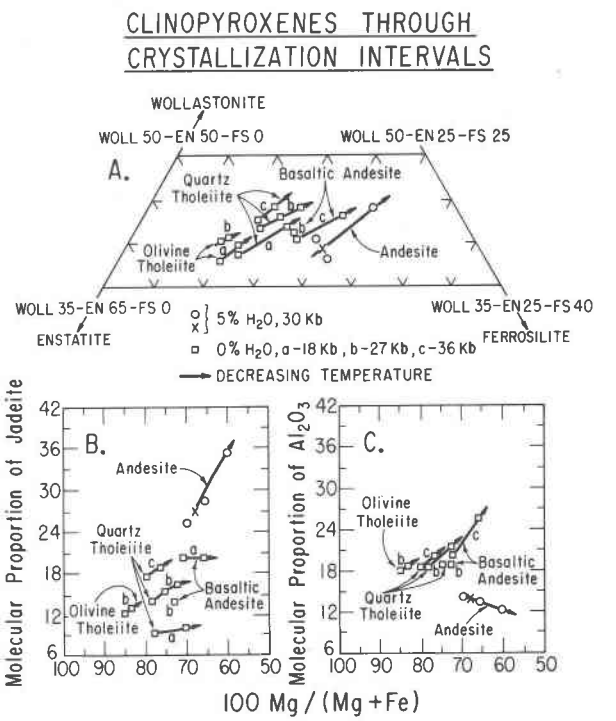

Fig. 7. Clinopyroxene compositions through the crystallization intervals of calc-alkaline liquids. Heavy arrows indicate decreasing temperature. Squares are for anhydrous liquids at 18 kbar (a), 27 kbar (b), and 36 kbar (c) from Green and Ringwood (1968). Circles are for andesite with 5 percent H_2O at 30 kbar (Table 4). The point x is the average composition of clinopyroxenes from different runs made at the same conditions.

The total Al_2O_3 in the clinopyroxenes increases with decreasing temperature (Table 4), despite the fact that the calculated Al_2O_3 proportion decreases in Figure 7C; the jadeite content increases to much higher levels than in the anhydrous, less siliceous liquids (Fig. 7B).

Liquids

Liquid compositions through the crystallization interval for andesite–H_2O were determined by analyses of quenched glasses with the electron microprobe. For those runs with only small amounts of interstitial liquid, satisfactory analyses were not possible. Liquids from the basaltic composition developed extensive quench clinopyroxene, which precluded useful analyses. H_2O-undersaturated liquids commonly quench to clear glasses at pressures below about 15 kbar (pressure varying with liquid composition and H_2O content). For runs at higher pressures, however, H_2O exsolves during the quench, expanding and cracking the glass and increasing the density differences between the experimental glasses and the standards used in analysis. In addition, the exsolved va-

Table 4. Compositions, determined by microprobe analysis, of clinopyroxenes in the melting interval of tonalite and gabbro at 30 kbar; with ΣFe = FeO

Composition	Tonalite 101						Gabbro DW-1	
Run #	408	409	314	316	329	308	411	412
Temp. °C	1100	1100	1000	1000	900	900	1200	1100
% H_2O	4	4	5	5	5	10	5	5
Capsule*	2	2	1	1	1	1	2	2
Time hr.	1	5	3	10	6	2	1	1
Co-existing Phases**	*Ga* Ky	*Ga* *Ky*	*Ga* Ky	*Ga* Ky	Ga Ky	Ga Ky	*Ga*	*Ga*
SiO_2	51.2	50.1	50.4	50.8	52.1	50.5	46.9	50.9
TiO_2	0.7	0.7	0.9	0.7	0.7	0.9	1.3	0.6
Al_2O_3	15.5	16.1	14.0	13.7	14.5	12.5	12.7	7.9
FeO	7.3	3.9	9.1	7.7	7.7	10.1	8.4	7.5
MgO	7.3	9.6	10.1	10.1	6.6	8.1	10.2	12.7
CaO	12.8	13.9	12.8	13.8	12.2	12.5	17.9	17.9
Na_2O	4.1	4.2	4.3	3.9	5.2	3.8	1.5	1.7
Total	98.9	98.5	101.6	100.6	99.0	98.4	98.9	99.2
Structural Formulae on the Basis of 6 Oxygens								
Si } Σ Z = 2	1.85	1.80	1.80	1.82	1.89	1.87	1.74	1.87
Al^{IV} } Σ Z = 2	.14	.19	.19	.17	.10	.13	.23	.12
Al^{VI}	.51	.49	.39	.40	.51	.41	.30	.22
Ti	.01	.01	.02	.01	.01	.02	.03	.01
Fe^{2+}	.22	.11	.27	.23	.23	.31	.26	.23
Mg	.39	.51	.54	.54	.35	.44	.56	.70
Ca	.49	.58	.49	.53	.47	.49	.71	.70
Na	.28	.29	.29	.27	.36	.27	.11	.11
Σ X + Y	1.93	2.02	2.02	2.00	1.96	1.96	1.99	1.99
Mol. Prop.***								
Wollastonite	24.0	26.6	22.4	24.6	23.2	24.0	32.7	32.1
Enstatite	19.1	23.5	24.6	25.1	17.4	21.6	25.7	31.8
Ferrosilite	10.8	5.4	12.4	10.7	11.4	15.1	11.9	15.0
Jadeite	27.6	26.7	27.3	25.4	35.7	26.0	10.2	10.8
Al_2O_3	18.3	17.7	13.3	14.2	12.3	13.2	19.4	10.3
Atomic Prop.								
Ca	44.6	48.0	37.7	40.8	44.7	39.5	46.5	43.2
Mg	35.3	42.4	41.4	41.5	33.3	35.6	36.6	42.7
Fe	20.1	9.6	20.9	17.7	22.0	24.9	16.9	14.1

*(1) $Ag_{30}Pd_{70}$. (2) $Ag_{75}Pd_{25}$.

**Liquid co-exists with all clinopyroxenes. Compositions of phases in italics have been determined.

***Al_2O_3 = (Σ Al − Na)/2; Jd = Na; Wo = Ca/2; En = Mg/2; Fs = Fe/2.

por may carry dissolved elements, especially alkalis, from the glass.

Ten individual areas of glass were analyzed for each run, using a scanning beam where possible. Reconnaissance studies indicated that the glasses were homogeneous. Oxide totals for analyses are 85–95 percent (Table 5). The low totals are caused by (1) H_2O dissolved in the glass, (2) the low density of the glasses compared to the standards used, and (3) alkali loss (especially Na_2O) during microprobe analysis.

Table 5. Compositions, determined by microprobe analysis, of glasses quenched from the melting interval of tonalite at 30 kbar, with ΣFe = FeO

Run #	310	318	346	314	316	329	306	343	307	361
Temp. °C	1175	1100	1100	1000	1000	900	1125	1000	950	1000
% H_2O	5	5	5	5	5	5	10	10	10	25
Capsule*	1	1	3	1	1	1	1	1	1	1
Time hr.	1	1	1	3	10	6	1	2	1	1
Co-existing Phases**	*Ga*	*Ga*	Ga	*Ga* *Cpx* Ky	*Ga* *Cpx* Ky	Ga *Cpx* Ky	*Ga*	*Ga*	Ga	*Ga*
SiO_2	58.3	59.4	60.8	62.7	63.6	65.8	55.1	61.6	60.9	58.3
TiO_2	0.6	0.7	0.7	0.6	0.6	0.3	0.8	0.6	0.5	0.7
Al_2O_3	16.9	16.6	17.1	14.8	15.1	13.1	17.0	16.5	16.2	17.1
FeO	3.1	2.5	0.9	1.2	0.9	0.6	4.1	1.5	1.5	3.1
(FeO)***	(3.9)***	(3.2)***	(3.2)***	(1.3)***	(1.2)***	(0.7)***	(5.2)***	(1.7)***	(1.7)***	(3.9)***
MgO	1.8	0.9	1.3	0.3	0.3	0.1	1.9	0.7	0.7	1.2
CaO	5.6	4.4	4.3	2.7	2.4	2.0	5.6	3.5	3.2	4.6
Na_2O	3.3	3.0	3.2	1.1	1.3	0.9	2.5	3.1	2.4	3.4
K_2O	2.1	2.1	2.3	2.9	2.8	2.7	2.2	2.5	2.6	2.1
Total	93.0	90.6	93.3	86.7	87.6	86.0	90.4	90.5	88.5	91.7
				Liquid Compositions with Σ Oxides = 100.0						
SiO_2	62.6	65.6	65.1	72.3	72.6	76.5	60.9	68.1	68.9	63.5
TiO_2	0.9	0.8	0.8	0.7	0.7	0.3	0.9	0.7	0.6	0.8
Al_2O_3	18.2	18.3	18.3	17.0	17.2	15.3	18.8	18.2	18.3	18.7
FeO	4.2	3.5	3.4	1.5	1.4	0.8	5.7	1.9	1.9	4.2
MgO	2.0	1.0	1.4	0.4	0.4	0.2	2.1	0.8	0.7	1.4
CaO	6.0	4.8	4.7	3.1	2.7	2.4	6.2	3.8	3.6	5.1
Na_2O	3.6	3.3	3.4	1.3	1.5	1.1	2.7	3.5	2.7	3.8
K_2O	2.3	2.3	2.4	3.4	3.2	3.1	2.4	2.7	2.9	2.3
Na_2O+K_2O	48.7	55.4	54.6	70.9	71.9	79.7	39.7	72.8	68.0	52.0
FeO	34.6	34.4	31.9	22.7	21.4	16.4	43.7	18.9	23.0	36.0
MgO	16.7	10.2	13.5	6.4	6.7	3.9	16.6	8.3	9.0	12.0
1/4 SiO_2	56.0	63.4	62.9	78.1	82.4	84.6	52.0	72.0	73.0	60.0
CaO	21.6	18.9	18.1	13.5	10.2	10.6	21.2	16.4	15.5	19.2
MgO+FeO	22.4	17.7	19.0	8.4	8.2	4.8	26.7	11.6	11.5	20.8

* (1) $Ag_{30}Pd_{70}$. (3) Pt.

** Phase in italics also analyzed.

*** (FeO) - Percentage iron after correction for iron loss to capsules.

With decreasing temperature through the crystallization interval of andesite with 5 percent H_2O (Fig. 2), the proportion of liquid decreases, and its H_2O content therefore increases; hence the oxide totals listed for analyses decrease.

All liquid compositions were corrected for loss of iron from the sample to the capsule, using correction factors determined by Stern and Wyllie (1975), then the oxide totals were normalized to 100.00. The normalized glass compositions for andesite–H_2O are listed in Table 5, and some of them are plotted in Figure 13.

Calculated phase compositions

Garnets and clinopyroxenes could be analyzed successfully only through limited temperature intervals

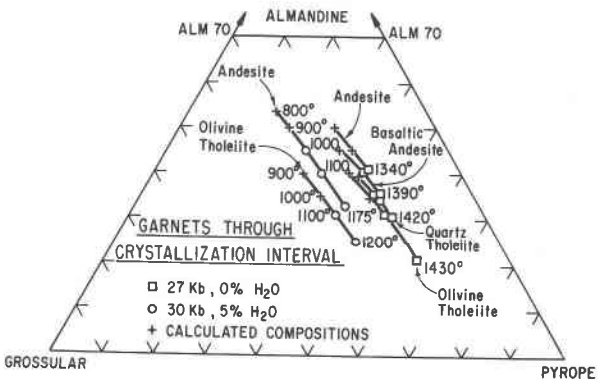

Fig. 8. Garnet compositions measured and calculated (crosses) through the crystallization intervals of calc-alkaline rock compositions. Squares are for garnets measured by Green and Ringwood (1968) in anhydrous liquids at 27 kbar (Figure 6); circles are for garnets measured in olivine tholeiite and andesite at 30 kbar with 5 percent H_2O. The values for hydrous andesite are the solid circles (averages) plotted in Figure 6A. The temperatures for plotted values through the crystallization intervals of anhydrous liquids are: olivine tholeiite, 1430°–1400°–1375°–1350°C; quartz tholeiite, 1420°–1400°–1385°–1350°; basaltic andesite, 1390°–1360°–1325°; andesites, 1340°–1320°–1300°. See Table 6 for calculated garnet compositions with 5 percent H_2O.

below the liquidus. For lower temperatures, compositions were calculated in two stages. First, the measured trends of mineral compositions shown in Figures 6 and 7 were extrapolated. Then, the amount of change in mineral compositions along these trends within a given temperature interval was calculated, based on (1) the measured compositional differences between minerals at known temperature intervals, and (2) the condition that at a given temperature the $K_D = (Fe/Mg)_{Ga}/(Fe/Mg)_{Cpx}$ of calculated garnet and clinopyroxene pairs equals the K_D of natural and experimental garnet–pyroxene pairs, at similar temperatures of final equilibration, as determined by Mysen and Heier (1972).

Glass compositions were measured only for liquids in the andesite composition. Liquid compositions through the crystallization intervals were calculated from the mineral compositions (measured and calculated), and the proportions of phases present at successive temperatures (measured or estimated).

Garnets

Figure 8 shows the measured (squares and circles) and calculated (crosses) compositions of garnets

Table 6. Calculated garnet compositions through the melting interval of tonalite and gabbro, with 5 weight percent water at 30 kbar

Composition	Tonalite 101 - 5% H_2O					Gabbro DW-1 - 5% H_2O			
Temp. °C	1175	1100	1000	900	800	1200	1100	1000	900
Mol. Prop.									
Grossular	26	27	28	29	30	28	29	30	31
Pyrope	41	33	27	21	12	47	40	35	29
Almandine	33	40	45	50	58	25	31	35	40
SiO_2	40.3	39.7	39.2	38.8	38.1	40.9	40.3	39.9	39.5
Al_2O_3	22.7	22.4	22.2	21.9	21.6	23.2	22.8	22.6	22.4
FeO = ΣFe	15.9	19.0	21.1	23.2	26.5	12.3	15.0	16.7	18.9
MgO	11.0	8.7	7.0	5.4	3.0	13.0	10.7	9.3	7.6
CaO	9.7	10.0	10.2	10.4	10.6	10.4	10.9	11.2	11.4
100 Mg/(Mg+Fe)	55.4	45.2	37.5	29.5	17.1	65.2	56.3	50.0	42.0
Fe/Mg	.800	1.21	1.67	2.38	4.83	.53	.78	1.00	1.38
(Fe/Mg)Cpx			.47	.70	.82	.30	.34	.40	.47
(K_D)			3.56	3.41	5.91	1.77	2.29	2.50	2.96
Oxide Prop.									
Na_2O+K_2O	0	0	0	0	0	0	0	0	0
FeO	59	68	74	81	89	48	58	64	71
MgO	40	31	25	18	10	51	41	35	28
1/4 SiO_2	21	20	20	19	19	22	21	21	20
CaO	20	21	21	21	21	22	23	23	23
MgO+FeO	57	58	58	58	59	55	55	55	55

through the crystallization intervals of four rock compositions studied dry at 27 kbar by Green and Ringwood (1968), and of our two rocks with 5 percent H_2O at 30 kbar. The mineral composition trends are selections from and extensions of the results in Figure 6. The temperatures of measured and calculated points are shown. The effect of bulk composition in this range is slight (compare Fig. 6B), but the effect of adding 5 percent H_2O to olivine tholeiite and andesite is larger (compare Figs. 5B and 6B). The oxide percentages of the garnets plotted in Figure 8 were calculated from the molecular proportions, and results for the two series with 5 percent H_2O are listed in Table 6.

Clinopyroxenes

Figure 9 shows the measured (circles and squares) and calculated (crosses) compositions of clinopyroxenes through the crystallization intervals of three rock compositions studied dry at 27 kbar by Green and Ringwood (1968), of our two rocks with 5 percent H_2O at 30 kbar, and a calculated point for dry andesite at 30 kbar. The mineral composition trends are selections from and extensions of the results in Figure 7. The calculated variations in Ca–Mg–Fe components determine the variation of jadeite and Al_2O_3 proportions.

The only reliable clinopyroxene analysis obtained at 30 kbar for olivine tholeiite with 5 percent H_2O plots in a reasonable position with respect to other analyses (Fig. 9A), and the trend is drawn through this point parallel to the others. Jadeite and Al_2O_3 proportions for this clinopyroxene are low (Figs. 9B and 9C), and the trends calculated for this crystallization interval are based on assumptions given in the legend for Figure 9. Because of the low molecular weight of Al_2O_3 compared with the other molecular components, the assumptions adopted have little effect on the compositions of calculated clinopyroxenes through this melting interval. Changing these trends would have little effect on the main conclusions of this work, which are illustrated in terms of ratios of the Ca–Mg–Fe components. These ratios are not affected by variation of Na and Al.

The effect of bulk composition on clinopyroxene compositions through the crystallization intervals (Fig. 9) is greater than that on garnet compositions (Fig. 8). The effect of adding 5 percent H_2O displaces the trends slightly in terms of Ca–Mg–Fe. For the andesite composition, the effect of 5 percent H_2O on jadeite and Al_2O_3 proportions is very marked, as

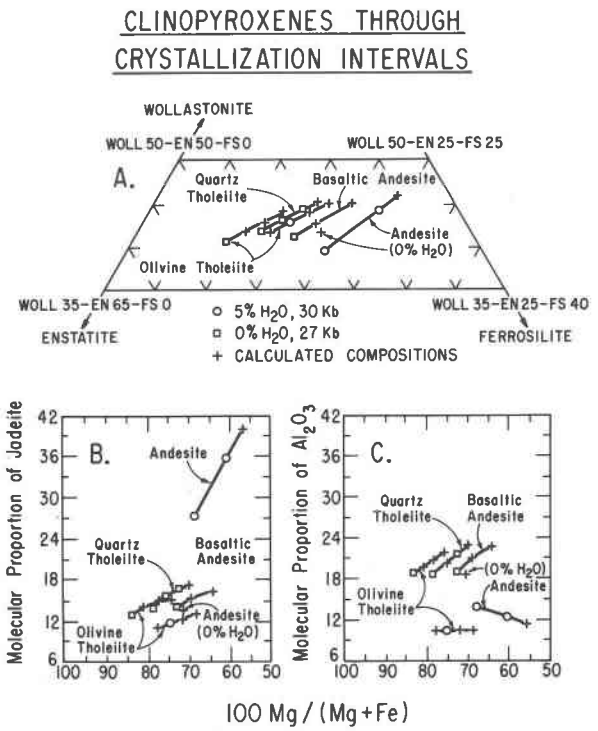

Fig. 9. Clinopyroxene compositions measured and calculated (crosses) through the crystallization intervals of calc–alkaline rock compositions. Squares are for clinopyroxenes measured by Green and Ringwood (1968) in anhydrous liquids at 27 kbar (see Fig. 7); circles are for clinopyroxenes measured in olivine tholeiite and andesite at 30 kbar with 5 percent H_2O. Jadeite and Al_2O_3 proportions for the clinopyroxene in hydrous olivine tholeiite at 30 kbar are low (compare Figs. 7B and C with 9B and C); the trend for jadeite is constructed parallel to those for clinopyroxene in anhydrous liquids; the Al_2O_3 proportion is assumed to be constant through the crystallization interval as a compromise between the increase for anhydrous liquids and the decrease for hydrous andesite. See Table 7 for calculated clinopyroxene compositions with 5 percent H_2O.

previously reviewed in connection with Figures 7B and C.

The oxide percentages of the clinopyroxenes plotted in Figure 9 were calculated from the molecular proportions, and results for the trends with 5 percent H_2O are given in Table 7. The temperatures of points plotted in Figure 9 can be obtained from corresponding points in Figure 8 and data listed in Tables 6 and 7.

Proportions of phases through crystallization intervals

Figure 10 shows the variation of weight percentages of phases through the crystallization interval of andesite with 5 percent H_2O at 30 kbar. The curves pass through values measured for five samples by point-counting polished run charges (prepared for

Table 7. Calculated clinopyroxene compositions through the melting interval of tonalite and gabbro, with 5 weight percent water at 30 kbar

Composition	Tonalite 101 5% H_2O			Gabbro DW-1 - 5% H_2O			
Temp. °C	1000	900	800	1200	1100	1000	900
Atomic Prop.							
Ca	37.7	44.7	47.0	41.5	43.0	44.0	45.0
Mg	41.4	33.3	30.0	45.0	42.5	40.0	37.5
Fe	20.9	22.0	23.0	13.5	14.5	16.0	17.5
Mol. Prop.							
Wollastonite	22.4	23.2	22.7	32.6	33.5	34.2	34.4
Enstatite	24.6	17.4	14.5	35.3	33.1	31.1	28.6
Ferrosilite	12.4	11.4	11.0	10.6	11.3	12.4	13.3
Jadeite	27.3	35.7	40.0	10.6	11.3	12.0	12.8
Al_2O_3	13.3	12.3	11.8	10.7	10.7	10.7	10.7
SiO_2	51.3	51.7	51.9	51.7	51.5	51.3	51.1
Al_2O_3	13.5	15.1	15.9	7.9	8.0	8.1	8.3
FeO	8.7	8.0	7.7	7.3	7.8	8.5	9.1
MgO	9.7	6.8	5.7	13.7	12.8	11.9	11.0
CaO	12.3	12.7	12.4	17.6	18.0	18.2	18.4
Na_2O	4.1	5.4	6.0	1.5	1.6	1.7	1.9
100 Mg/(Mg+Fe)	66.5	60.3	56.6	76.9	74.6	71.4	68.2
Fe/Mg	.47	.70	.82	.30	.34	.40	.47
(Fe/Mg)Ga	1.67	2.38	4.83	.53	.78	1.00	1.38
K_D	3.56	3.41	5.91	1.77	2.29	2.50	2.96
Oxide Prop.							
Na_2O+K_2O	18	26	31	7	7	8	8
FeO	38	39	39	32	35	38	41
MgO	43	33	29	60	57	53	49
1/4 SiO_2	29	31	33	25	25	24	24
CaO	28	31	32	34	35	35	35
MgO+FeO	42	36	34	40	40	39	39

microprobe analysis) under reflected light. Approximately 1200 points were counted for each sample. Volume percentages were then converted to weight percentages, using densities given in the legend (Table 8). The liquid curve is further constrained by the points at the liquidus and solidus temperatures, determined independently (Fig. 2).

The proportions of mineral phases through the crystallization interval of olivine tholeiite with 5 percent H_2O (Table 8) were estimated by examination of crushed fragments mounted in immersion oils (transmitted light). The phase assemblages are simple (Fig. 3), but these estimates, complicated by development of quench clinopyroxene in near-liquidus runs, are much less reliable than values plotted in Figure 10.

Green and Ringwood (1968) estimated proportions of phases below the liquidi at 27 kbar for anhydrous olivine basalt, quartz tholeiite, basaltic andesite, and andesite. We have extrapolated these values through the crystallization intervals; the temperature intervals are about 100°C, contrasted with 400–500°C if 5 percent H_2O is present (Figs. 2 and 3). Despite the narrow temperature interval involved, there is obviously scope for significant error in the modes adopted for the lower temperatures.

The calculated compositions of liquids are plotted in Figures 11 and 12, along with the compositions and proportions of garnet and clinopyroxene through the crystallization intervals. They are compared with the dashed line representing the average chemical variation trend for calc-alkaline rocks, from Figure 1. Errors in estimates of modes through the crystallization interval produce errors in the calculated liquid paths, but it will be shown below that these errors do not invalidate the petrological conclusions drawn from the liquid paths.

Compositions of anhydrous liquids

Figures 11A and B show the calculated equilibrium liquid path through the crystallization interval for anhydrous olivine tholeiite at 27 kbar, together with coexisting garnet and clinopyroxene. The values for 1430°C (number 1) are from Green and Ringwood (1968, Figure 10, Table 16). Calculated values for 1400°C (number 2) differ from those of Green and Ringwood (1968), because they used a clinopyroxene composition from the melting interval of quartz tholeiite, and we used a composition calculated for olivine tholeiite (see Fig. 9). Our calculations extend the liquid path to lower temperatures than those of Green and Ringwood.

With decreasing temperature, the composition of

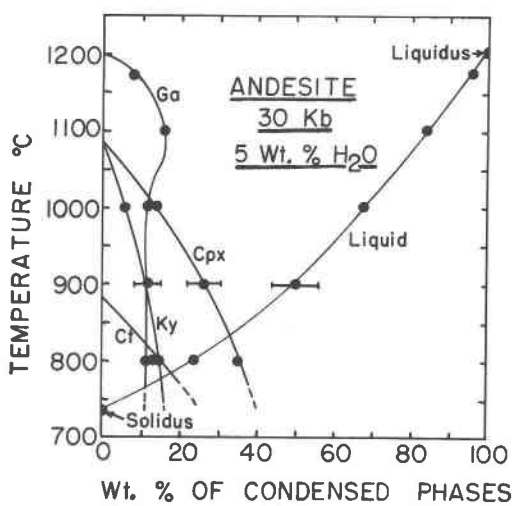

Fig. 10. The weight percentage of condensed phases through the melting interval of andesite with 5 percent water at 30 kbar (Fig. 2). Volume percentages determined by point-counting were converted to weight percentages using the following densities: $\rho_{kyanite} = 3.60$; $\rho_{coesite} = 3.01$; $\rho_{glass} = 2.6$; $\rho_{cpx} = 3.40$; $\rho_{garnet} = 4.00$. Brackets at 900°C indicate range of error for 1000 counts (Van der Plas and Tobi, 1965). Abbreviations, see Fig. 2.

the remaining liquid changes relative to the average calc–alkaline trend (the dashed line, from Fig. 1): Fe/Mg increases sharply due to the low Fe/Mg of the clinopyroxene (Fig. 11A), and Ca/(Mg + Fe) increases due to low Ca/(Mg + Fe) of garnet.

The effect of errors in modal estimates is illustrated by points 5 and 6 for 1400°C and 1375°C, respectively. These points are calculated for bulk mineral compositions with a higher proportion of garnet. The proportion is adjusted to reduce Fe/Mg in calculated liquids so that they coincide with the average calc–alkaline trend. This adjustment increases the divergence of the calculated liquid path from the calc–alkaline trend in terms of Ca/(Mg + Fe), as shown in Figure 11B.

Figure 11C and D show the calculated equilibrium liquid paths through the crystallization intervals for anhydrous quartz tholeiite, basaltic andesite, and andesite at 27 kbar, extending the near-liquidus data of Green and Ringwood (1968) to lower temperatures.

Table 8. Calculated liquid compositions, and compositions of bulk crystal phases, through the melting interval of tonalite and gabbro, with 5 weight percent water at 30 kbar

Composition	Tonalite 101 - 5% H_2O					Gabbro DW-1 - 5% H_2O			
Temp °C	1175	1100	1000	900	800	1200	1100	1000	900
% Liquid	92	84	68	50	24	80	60	40	20
% Ga	8	16	12	12	12	10	14	21	25
% Cpx			14	26	35	10	26	39	50
% Ky			6	12	14				5
% Ct(qz)					15				
Liquid Compositions									
SiO_2	62.4	64.6	68.4	76.2	73.4	48.4	48.1	48.8	62.3
Al_2O_3	18.3	17.9	15.2	9.1	7.0	18.5	21.1	25.0	22.7
FeO = Σ Fe	4.9	3.3	3.0	1.9	0.5	10.3	10.1	8.4	2.3
MgO	1.8	1.3	0.5	0.2	0.7	6.4	4.9	2.9	0.2
CaO	5.7	5.3	4.5	2.9	1.7	14.1	13.1	11.7	7.9
Na_2O	4.2	4.6	4.8	5.0	7.0	1.9	2.2	2.5	3.6
K_2O	2.4	2.6	3.3	4.5	9.2	0.1	0.2	0.3	0.7
Oxide Prop.									
Na_2O+K_2O	49	58	69	81	92	11	14	20	63
FeO	36	29	26	16	3	54	57	58	34
MgO	13	12	4	2	4	34	28	20	3
1/4 SiO_2	55	61	67	78	85	28	29	34	59
CaO	20	20	18	12	8	32	32	33	30
MgO+FeO	24	18	14	9	6	38	37	32	9
Compositions of Bulk Crystal									
SiO_2	40.3	39.7	44.1	45.0	56.5	46.3	47.6	47.1	44.5
Al_2O_3	22.7	22.4	26.0	23.2	22.4	15.5	13.2	13.1	16.8
FeO	15.9	19.0	11.7	9.7	7.5	14.2	15.5	15.7	12.1
MgO	11.0	8.7	6.9	4.8	3.1	13.4	12.1	11.0	9.6
CaO	9.7	10.0	9.2	9.1	7.4	9.8	10.3	11.3	15.6
Na_2O	0.0	0.0	1.8	2.8	2.8	0.8	1.1	1.1	1.2
Oxide Prop.									
Na_2O+K_2O	0	0	8	16	20	2	3	4	5
FeO	59	68	57	55	55	49	54	56	52
MgO	40	31	33	27	23	47	42	39	42
1/4 SiO_2	21	20	28	32	43	23	23	23	22
CaO	20	21	23	26	23	20	20	23	23
MgO+FeO	57	58	48	41	33	56	55	53	44

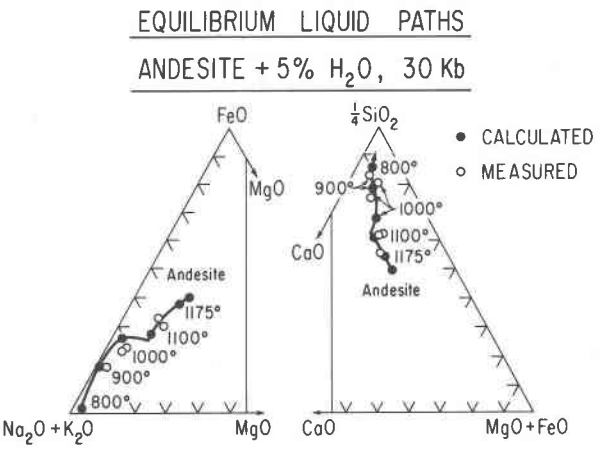

Fig. 11. Calculated liquids through the crystallization intervals of anhydrous compositions at 27 kbar. Near-liquidus data (olivine tholeiite, 1430°C; quartz tholeiite, 1420°–1400°–1385°C; basaltic andesite, 1390°–1360°C; and andesite, 1340°C) are from Green and Ringwood (1968, Fig. 10, Tables 16, 17, and 18). Coexisting minerals (Figs. 8 and 9 and Tables 6 and 7) are connected by tie-lines. The dashed line is the average calc–alkaline trend from Fig. 1. (A) and (B) show the equilibrium liquid paths for anhydrous olivine tholeiite. The temperatures of numbered points are: (1) 1430°, (2) 1400°, (3) 1375°, (4) 1350°C. Points 5 and 6 at 1400° and 1375°C, respectively, are calculated liquid compositions for modes with higher garnet/clinopyroxene. (C) and (D) show equilibrium liquid paths for anhydrous quartz tholeiite (calculated at 1420°–1400°–1385°–1350°C), basaltic andesite (calculated at 1390°–1360°–1325°C), and andesite (calculated at 1340°–1320°C).

The temperatures of points from Green and Ringwood (1968, Fig. 10, Tables 17 and 18) and of points calculated from the mineral data in Figures 8 and 9 are listed in the figure legend. The liquid paths correspond fairly closely with the average trend of calc–alkaline rocks with respect to Fe/Mg (Fig. 11C), but with decreasing temperature there is a progressive increase in Ca/(Mg + Fe) relative to the rock trend (Fig. 11D), with divergence less for andesite than for basalt.

Compositions of hydrous liquids

Figure 12 shows the calculated equilibrium liquid paths through the crystallization intervals for olivine tholeiite and andesite with 5 percent H_2O at 30 kb (Figs. 2 and 3), together with the compositions of coexisting garnet and clinopyroxene. The numerical data listed in Table 8 incorporate the modal results for andesite from Figure 10 and estimated modes for basalt. Numbers identify the coexisting liquids and crystals at temperatures from 1200° (1) to 900°C (4) for the olivine tholeiite in Figures 12A and B, and from 1175° (1) to 800°C (5) for the andesite in Figures 12C and D. The temperatures of other points are given in the figure legend.

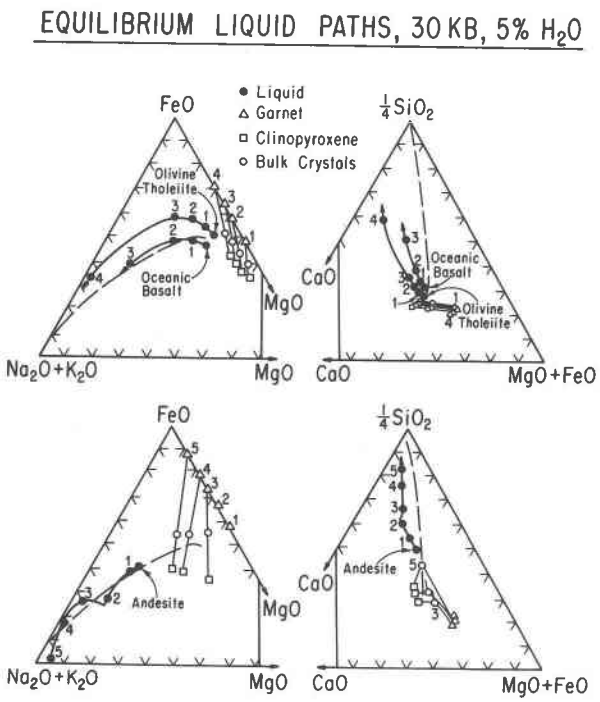

Fig. 12. Calculated liquid compositions through the crystallization intervals of basalt and andesite with 5 percent H_2O at 30 kbar. Liquid and bulk crystalline phase compositions for the olivine tholeiite and andesite are given in Table 8. Coexisting minerals (from Figs. 8 and 9 and Tables 6 and 7) are connected by tie-lines; coexisting liquids and bulk crystal assemblages are labeled with small integers. The dashed line is the average calc–alkaline composition trend (Fig. 1). (A) and (B) show the equilibrium liquid paths for an olivine tholeiite and oceanic abyssal basalt with 5 percent H_2O. Liquids were calculated at (1) 1200°, (2) 1100°, (3) 1000°, (4) 900°C. (C) and (D) show the equilibrium liquid path for an andesite with 5 percent H_2O. Liquids were calculated at (1) 1175°, (2) 1100°, (3) 1000°, (4) 900°, (5) 800°C.

The liquid path for hydrous olivine tholeiite in Figures 12A and B (points 1–4) follows a trend similar to that for anhydrous olivine tholeiite in Figures 11A and B (points 1–4), but the increase in Ca/(Mg + Fe) is much greater for the hydrous tholeiite. Considering applications of these results, we may argue that the basaltic composition used (gabbro DW-1, Table 1) differs from abyssal oceanic basalt, and therefore is not a useful model for subducted oceanic crust. A liquid path has been calculated by subtracting the same mineral assemblages at 1200°, 1100°, and 1000°C (curves 1–3 in Figs. 12A and B) from an average abyssal oceanic basalt (Engel *et al.*, 1965). Although it is unlikely that minerals of these exact compositions would be in equilibrium with liquids through the crystallization interval of the oceanic basalt, the equilibrium phase compositions would be in the same range (Figs. 8 and 9).

The calculated liquid path for the hydrous oceanic basalt is close to the average calc–alkaline rock trend with respect to Fe/Mg, in contrast to the path for hydrous olivine tholeiite (Fig. 12A). It is closer to the average rock trend with respect to Ca/(Mg + Fe) than that for the hydrous tholeiite, but still it diverges significantly, with increasing Ca/(Mg + Fe) at lower temperatures (Fig. 12B).

We noted above that corrections for iron loss to the capsule were not made for clinopyroxenes (Fig. 7). If a correction had been applied, addition of iron to the bulk mineral assemblage in Figures 12A and B would have decreased the iron content of calculated liquids, reducing their Fe/Mg, and bringing the liquid path for hydrous olivine tholeiite closer to the calc–alkaline rock trend in Figure 12A. However, this correction would also lower Ca/(Mg + Fe) of the bulk crystal assemblage, and increase the divergence between the calculated liquid path and the average rock trend in Figure 12B.

The crystallization path for andesite with 5 percent H_2O at 30 kbar is more complex than those reviewed above, as shown by the successive phase fields intersected in Figure 2 (see Fig. 10). Garnet is the only mineral crystallizing for about 100°C below the liquidus. For temperatures of 1175° and 1100°C (points 1 and 2, respectively), the high Fe/Mg of garnet maintains the liquid composition close to the average calc–alkaline rock trend in Figure 12C, but the low Ca/(Mg + Fe) of garnet drives the liquid path away from the average rock trend in Figure 12D. With the appearance of clinopyroxene and kyanite just below 1100°C (Figs. 2 and 10), continued crystallization causes an increase in Fe/Mg and constancy of Ca/(Mg + Fe) in the liquids.

Figure 12D shows great enrichment of the remaining liquid in SiO_2, which may exceed 75 percent (Table 8, 1000° and 900°C). Below 900°C quartz crystallizes, followed by coesite (Figs. 2 and 10), but the SiO_2 content of the calculated liquid remains greater than 73 percent (Table 8, 800°C). Figure 12C shows in addition very high (Na + K)/(Mg + Fe) in the low-temperature liquids for hydrous andesite, compared with liquids in hydrous basalts (Fig. 12A). We detected no potassic minerals in the runs, despite the high K_2O content in calculated liquids (Table 8, 4.5 percent at 900°, 9.2 percent at 800°C). At temperatures where vapor is present (Fig. 2), K_2O is strongly partitioned into the vapor (Boettcher and Wyllie, 1968; Stern, 1973).

The H_2O contents of liquids plotted in Figure 12 increase from 5 percent at the liquidus to saturation

values near 22.5 percent a few degrees above the solidus, that is, about 760°C for andesite (Fig. 2) and about 780°C for tholeiite (Fig. 3). For the andesite, Figure 10 shows that at 900°C there is 50 percent liquid, which must contain 10 percent H_2O, and at 800°C the 24 percent liquid must contain about 20 percent H_2O.

Measured and calculated liquid compositions

Figure 13 compares the measured (Table 5) and calculated (Figs. 12C and D, Table 8) liquid compositions through the crystallization interval of andesite with 5 percent H_2O at 30 kbar. The measured compositions agree closely with the liquid paths defined by the calculated liquids, although there are differences in elemental ratios at 1100° and 1000°C in the FAM diagram, and at 1000° and 900°C in the SiO_2 diagram.

The differences can be examined in detail from the normalized analyses listed in Tables 5 and 8. There is good agreement at 1175° and 1100°C, with discrepancies from some oxides becoming significant at 1000° and 900°C. At all temperatures, the Na_2O contents of measured glasses are lower than calculated values, due to volatilization of Na during probe analysis, and perhaps enhanced by loss of Na+K dissolved in the aqueous vapor which escapes from the liquid and glass during quenching. The measured K_2O is lower than the calculated value at 900°C. If correction factors could be applied for Na_2O lost during microprobe analysis, values for all other oxides in the renormalized measured analyses would be somewhat reduced, but not sufficiently to modify the following comparisons.

Measured values of total iron drop to about half of the calculated values at 1000° and 900°C. The measurements were corrected for iron loss following Stern and Wyllie (1975), but perhaps the correction factors applied were too low for these temperatures (see Table 5). At 1000°C the measured SiO_2 is somewhat higher and the measured CaO is somewhat lower than the calculated values. Measured Al_2O_3 is slightly higher than the calculated value at 1000°, and very much higher at 900°C (15.3 percent compared with 9.1 percent). The calculated Al_2O_3 at 800° is even lower than that at 900°C (7.0 percent). Such a large discrepancy in Al_2O_3 suggests that the modal proportion of kyanite may have been overestimated (Fig. 10). This is the only sequence of runs in which kyanite is significant.

No quench crystals were observed in runs with the tonalite, but growth of minerals on the surfaces of primary grains during the quench, although difficult to detect, could cause large changes in the compositions of quenched glasses, as pointed out by Green (1973) for clinopyroxene. There are no consistent differences between measured glass and calculated liquid compositions that could be caused by the growth of minerals during the quench, so we conclude that this is not a problem for andesite with 5 percent H_2O.

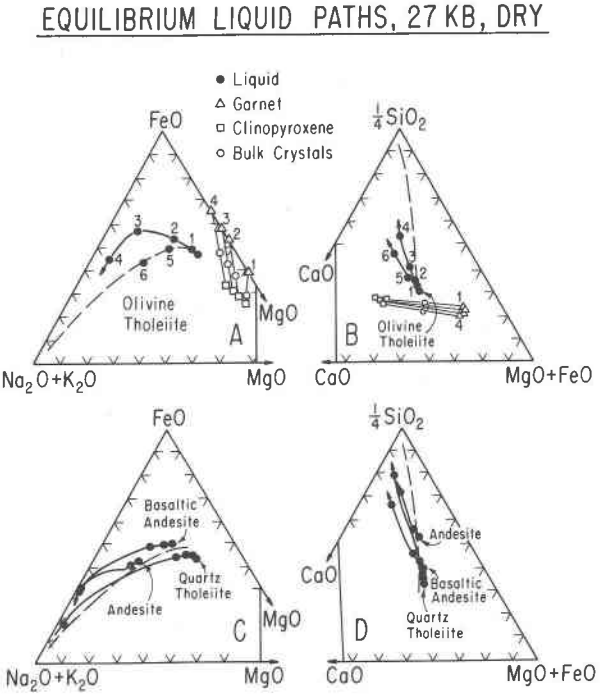

Fig. 13. Comparison of calculated (closed circles) and measured (open circles) liquid compositions through the crystallization interval of andesite with 5 percent H_2O at 30 kbar. Calculated liquids and liquid path are transferred from Figs. 12C and 12D and Table 8; measured glasses are listed in Table 5.

These results indicate that the calculated liquids for the other compositions are reasonably reliable. Additional errors are introduced into the other calculated liquid sequences, however, because the estimates of phase proportions are less certain.

Petrological applications

The calc–alkaline igneous rocks lie in a complex system, needing ten or more major components for their definition. The lines in Figure 1 show the average chemical variation of the rocks in terms of six components. The line in Figure 1B, reproduced as the dashed line in Figure 14, shows the average trend in terms of three variables, with SiO_2 as the main one. The calc–alkaline rock compositions studied by

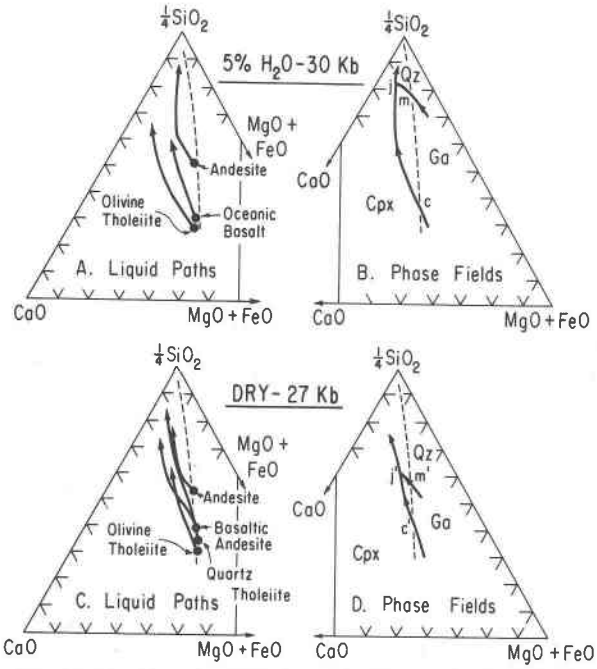

Fig. 14. Liquidus phase relations with 5 percent H_2O at 30 kbar, and dry at 27 kbar. Dashed lines show the average calc-alkaline compositional trend from Fig. 1B. (A) The calculated equilibrium liquid paths with 5 percent H_2O at 30 kbar from Figs. 12B and D. (B) A schematic pseudoternary liquidus phase diagram with 5 percent H_2O at 30 kbar. Points *m* and *c* are piercing points from Fig. 4. For details see text. (C) The calculated equilibrium liquid paths at 27 kbar from Figs. 11B and D (anhydrous). (D) A schematic pseudoternary liquidus phase diagram at 27 kbar. Points *m'* and *c'* are piercing points from Fig. 4. For details see text.

Green and Ringwood (1968, 1972) and Green (1972), and the gabbro–tonalite–granite series that we have used (Table 1; Stern and Wyllie, 1973), plot very close to this average trend line. We will assume that the composition join basalt–andesite–rhyolite of Figure 4 is coincident with the dashed line in Figure 14.

Green and Ringwood (1968) and Green (1972) applied their results for this composition join in the range 27–36 kbar to magmatic processes in and above subducted ocean crust, concluding that liquids derived from partial fusion of quartz eclogite or crystallization of basaltic liquids broadly follow the calc-alkaline trend. They discussed sequences of crystallization and fusion as if the phase fields intersected by their bulk compositions were binary, or nearly so. Stern and Wyllie (1973) pointed out that the basalt–andesite–rhyolite join of Figure 4 is a section through a complex system, and they argued that, with crystallization, liquid compositions must diverge from the join. They emphasized the need to establish the extent of this divergence. We can now re-examine the conclusions with the data in hand.

Equilibrium liquidus paths and field boundaries

The calculated equilibrium liquid paths for hydrous compositions have been transferred to Figure 14A from Figure 12, and for anhydrous compositions to Figure 14C from Figure 11. Each liquid path, representing the passage of a fixed bulk composition through phase fields such as those in Figures 2 and 3, traces the composition of the liquid across liquidus surfaces and along field boundaries.

The phase relationships such as those illustrated in Figures 2, 3, and 4 can be represented as projections into a pseudoternary system. The liquid paths in Figures 14A and C are used to distinguish liquidus areas for the primary crystallization of clinopyroxene, garnet, and quartz, and the approximate positions of field boundaries between them, as shown in Figures 14B and D. We are dealing with a hyperdimensional system projected into a triangle, and the individual liquid paths do not coincide precisely along ternary field boundaries. They occupy zones that delineate the patterns shown in Figures 14B and D.

Figure 4 shows liquidus profiles for the basalt–andesite–rhyolite join in the presence of fixed amounts of H_2O. For the anhydrous join, there are two piercing points on the liquidus, *c'* and *m'*, which have been transferred to Figure 14D. For the join with 5 percent H_2O the liquidus profile is situated at lower temperatures, and the corresponding piercing points are *c* and *m*; these have been transferred to Figure 14B.

Phase relationships with 5 percent H_2O at 30 kbar. In the presence of 5 percent H_2O, Figure 14B shows a clinopyroxene–garnet field boundary and a garnet–quartz field boundary crossing the basalt–andesite–rhyolite join at piercing points *c* and *m*, respectively. The approximate extent of the garnet liquidus area is shown by the point where the andesite liquid path changes direction (Fig. 14A), which is where garnet is joined by clinopyroxene near 1100°C (Fig. 2). The position of the clinopyroxene–garnet field boundary in Figure 14B is based on the liquid path for oceanic basalt and the portion of the andesite path below 1100°C (Fig. 14A). In the complex rock system, the clinopyroxene–garnet field boundary would occupy a zone in Figure 14, because there are more variables for basalt and clinopyroxene–garnet compositions than can be represented in this triangle. The possible extent of the zone is indicated by the different paths for oceanic basalt and olivine tholeiite in Figure 14A. The arrangement in Figure 14B is probably near the lower limit for the extent of the garnet liquidus field, with 5 percent H_2O. This brings the pseudoternary

field boundary as close as possible to the basalt-andesite–rhyolite join. The crystallization of accessory kyanite is not represented (see Figs. 2, 3, and 10).

With 5 percent H_2O, clinopyroxene and garnet are joined by quartz or coesite at 900°C for the andesite (Figs. 2 and 10) and near 800°C for the olivine tholeiite (Fig. 3). The position of the garnet–quartz field boundary, intersecting the basalt–andesite–rhyolite join at an oblique angle, is based on the fact that point *m* at 1050°C contains about 71 percent SiO_2 (Fig. 4), and point *j* representing liquid in andesite near 900°C contains 76 percent SiO_2 (Tables 5 and 8). With continued crystallization of clinopyroxene+garnet+quartz (*j* is not a ternary reaction point), the liquid is enriched in Si/(Ca+Mg+Fe) as shown in Figure 14B, although the precipitation of quartz (or coesite) may halt the absolute enrichment of liquid in SiO_2 (Table 8). The dominant change at the lower temperatures is the enrichment of liquid in alkalis (Figs. 12A and C, Table 8), which is not represented in Figure 14.

For initial liquids with compositions in the range andesite–basalt, the point *j* would actually be represented by a zone extending from *j* towards CaO, with decreasing temperature corresponding to the lower temperature of appearance of quartz or coesite (compare Figs. 2 and 3). Figure 14B represents the most favorable pseudoternary phase diagram with respect to proximity of basalt liquid paths to the basalt–andesite–rhyolite join.

Anhydrous phase relationships at 27 kbar. Figure 14D represents the most favorable anhydrous pseudoternary phase diagram with respect to proximity of basalt liquid paths to the basalt–andesite–rhyolite join. It is based on the calculated liquid paths plotted in Figure 14C, which extend the results of Green and Ringwood (1968) and Green (1972), and following the considerations reviewed above for construction of Figure 14B.

The clinopyroxene–garnet field boundary passing through *m'* remains closer to the composition join, and the garnet field is smaller than in the hydrous system in Figure 14B (see *c'm'* in Fig. 4). This boundary represents the edge of the zone of hyperdimensional field boundaries in the complex system for basic calc–alkaline rocks, nearest to the composition join.

Calculated liquids coexisting with garnet and clinopyroxene may contain more than 65 percent SiO_2 (data not tabulated), and the point *m'* contains 63 percent SiO_2 (Fig. 4). Therefore, the garnet–quartz field boundary intersects the join obliquely, with the point of intersection of the field boundaries marking the precipitation of quartz, *j'*, containing more than 65 percent SiO_2. The coprecipitation of quartz at temperatures below *j'* reduces the absolute enrichment of remaining liquid in SiO_2, although Si/(Ca+Mg+Fe) may still increase along with alkali enrichment.

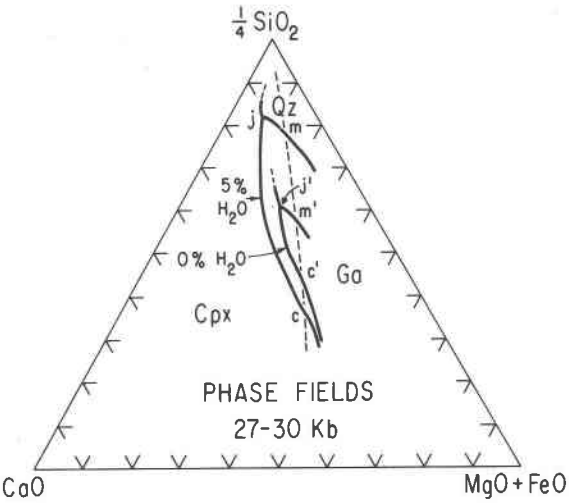

Fig. 15. Pseudoternary phase diagram showing effect of 5 percent H_2O on liquidus field boundaries (from Figs. 14B and D). Points labelled *c*, *m*, *c'*, and *m'* are from Fig. 4. The dashed line shows the average calc–alkaline composition trend from Fig. 1B, which is almost coincident with the basalt–andesite–rhyolite join of Fig. 4.

Equilibrium paths of crystallization and fusion

Figure 15 compares the pseudoternary liquidus surfaces for calc–alkaline rock compositions from Figures 14D (anhydrous) and 14B (with 5 percent H_2O). The 3 kbar pressure difference is not significant compared with the effect of 5 percent H_2O (Figs. 5, 6, and 7). None of the equilibrium liquid paths correspond precisely with the average basalt–andesite–rhyolite join. Crystallizing liquids are progressively enriched in Ca/(Mg+Fe) compared with this join. The divergence is small for anhydrous compositions, and larger with increasing H_2O. The corresponding changes in Fe/Mg/(Na+K) can be seen from comparison of Figure 14 with Figures 11 and 12.

We have considered the effects of errors in modal estimates and iron correction factors, and found that adjustments of these to bring the liquid paths into coincidence with the rock join in one projection (*e.g.* Fig. 12A) increase the path divergence in the other projection (*e.g.* Fig. 12B).

Crystallization of anhydrous basalt at 100 km

depth. Green and Ringwood (1968) calculated liquid compositions produced by equilibrium crystallization of up to 35 percent of four calc–alkaline rock compositions, and showed that these liquids broadly followed the chemical variation trend of the Aleutian Island calc–alkaline province, plotted on a FAM diagram. They suggested that about 50 percent crystallization of an anhydrous basaltic liquid would produce an andesite, and concluded that the thermal valley in the anhydrous liquidus profile, represented in Figure 4 as $c'm'$, would prevent fractionation to liquids more SiO_2-rich than andesite. This argument implies that the thermal minimum is a terminus for crystallizing liquids, as it would be if the composition join were a binary system.

Extension of Green and Ringwood's (1968) calculations beyond 35 percent crystallization shows that although equilibrium liquid paths remain fairly close to the average calc–alkaline trend in terms of FAM components (Fig. 11C), the liquids are enriched in Ca/(Mg + Fe) compared with the average rock trend (Fig. 4C). The lowest temperature in the thermal valley for the dry profile in Figure 4 is about 1390°C; the solidus where equilibrium crystallization terminates is lower by 60–70°C, according to Figure 3. Liquids similar to andesites in terms of SiO_2 content represent just one group in a continuous range of compositions extending to liquids with more than 65 percent SiO_2. The compositions of near-solidus liquids from anhydrous basalts are still inadequately determined, but enrichment in alkalis is anticipated (Green and Ringwood, 1968).

Partial melting of anhydrous quartz eclogite at 100 km depth. Ringwood (1975, p. 269) reviewed the Canberra experimental program, and concluded that from anhydrous quartz eclogite: "With a moderate degree of partial melting, an andesite magma could be formed. . . . The magma will not move from the andesite minimum until all of the quartz in the parental quartz eclogite has been incorporated into the liquid. Then, with greater degree of melting, basaltic andesite might be formed." According to Green and Ringwood (1968), 40–50 percent melting produces andesitic liquid.

In fact, there is no andesite minimum controlling the liquid composition, as shown by the paths for equilibrium fusion represented schematically in Figures 14D and 15. Melting progresses through about 30°C (Fig. 3) along a field boundary for quartz, clinopyroxene, and garnet until liquid reaches the composition j', where the last of the quartz disappears; then fusion continues along the garnet–clinopyroxene field boundary $j'c'$. Liquids similar to andesites in terms of SiO_2 content represent just one group in a continuous range of compositions.

Temperatures required to reach the liquidus of anhydrous andesitic compositions approach 1400°C (Fig. 2 and 4). These temperatures are higher than most estimates in a subduction zone at 100 km depth (Wyllie, 1973).

Partial melting of hydrous quartz eclogite at 100 km depth. Green and Ringwood (1972) and Green (1972) found, consistent with our results in Figure 4, that the thermal valley in the liquidus profile for the basalt–andesite–rhyolite join was shifted from andesite (m') to dacite or rhyodacite ($m'm$) in the presence of H_2O. On this basis, they concluded that dacite or rhyodacite liquids may be produced by partial melting of hydrous quartz eclogite at 100 km depth. This conclusion would be strictly valid only if the composition join approximated a binary system. We interpret this thermal valley as a piercing point for a garnet–quartz field boundary, and Figures 14B and 15 show that average dacites and rhyolites are not among liquids produced by partial fusion of hydrous quartz eclogite.

Figure 4 shows that the solidus temperature for quartz eclogite in the presence of H_2O is 250°C below the liquidus minimum with 5 percent H_2O, and 400°C lower with 2 percent H_2O. This is quite inconsistent with binary phase relationships. The path of equilibrium fusion for quartz eclogite in the presence of a fixed amount of H_2O can be traced on Figure 3, with the liquid compositions changing as represented in Figures 14 and 15. For 5 percent H_2O, melting begins at a temperature near 750°C. Within a few tens of degrees, all vapor and coesite dissolve, and the liquid passes the point corresponding to j in Figure 14B. At 900°C the liquid contains 62.3 percent SiO_2 (calculated, Table 8). Kyanite disappears near 1000°C, where the liquid contains 49 percent SiO_2, and garnet and clinopyroxene then melt together with increasing temperature. Figure 14A shows that, for a quartz eclogite, the point where coesite/quartz disappear is more enriched in Ca/(Mg+Fe) than the corresponding point j in Figure 14B.

For a more realistic situation, with a smaller amount of H_2O, the pseudoternary phase diagram would be intermediate between the two shown in Figure 15. The paths followed by liquids during equilibrium fusion are similar during the initial stages to those for 5 percent H_2O, but they are greatly extended in terms of temperature, as shown in Figure 3 (*e.g.* quartz remains to a much higher temperature),

and the later states of fusion approach those in the anhydrous system.

For H_2O contents below 1 percent, Figure 3 shows that all H_2O dissolves near the solidus, producing H_2O-saturated liquid (about 22.5 percent H_2O). With increase in temperature, H_2O-undersaturated liquid persists with coesite/quartz, kyanite, garnet, and clinopyroxene, increasing in amount slowly (with concomitant decrease in H_2O content) through a wide temperature interval. The temperature at which all quartz dissolves depends critically on the H_2O content (and the phase boundaries, which are not closely defined). Quartz could persist to 1000°, 1100°, or 1200°C, to a point on an H_2O-dependent boundary corresponding to *jj'* (Figs. 14 and 15). At higher temperatures, the liquid coexisting with garnet and clinopyroxene (±kyanite) follows the equivalent of a field boundary between *jc* and *j'c'*.

The compositions of hydrous liquids coexisting with quartz eclogite along the field boundary below *jj'*, before all quartz melts (Fig. 3), are certainly richer in SiO_2 than andesite, and probably greatly enriched in alkalis (Fig. 12A) and incompatible elements (compare results for tonalite in Tables 5 and 8). According to Figures 14A and 15, they are also considerably enriched in Ca/(Mg+Fe) compared with the average dacites and rhyodacites.

Effect of pressure. Figures 5 and 7A show that, with increasing pressure, Ca/(Mg+Fe) increases in garnets and clinopyroxenes, which would reduce Ca/(Mg+Fe) in liquid paths if the proportions of minerals through the crystallization interval remained the same. At higher pressures, the liquids would then approach more closely the average calc–alkaline join in Figure 14. However, this effect is offset by the increasing garnet/clinopyroxene reported with increasing pressure in the crystallization intervals of anhydrous basalt and andesite, and hydrous andesite (Green and Ringwood, 1968; Green, 1972).

Fractional crystallization and fusion

Green and Ringwood (1968) and Green (1972) determined equilibrium liquid paths and related them to fractional processes. They referred to fractional crystallization and "liquid fractionates" from rocks, without distinguishing between equilibrium and fractionation paths. For minerals with solid solution, it is not valid to equate fractionation with equilibrium paths. Equilibrium fusion is the reverse of equilibrium crystallization, but processes of fractional fusion and fractional crystallization yield products distinctly different from each other, as well as from the products of equilibrium processes, as demonstrated for fusion by Presnall (1969). Stern and Wyllie (1973) outlined the effect of fractional fusion on quartz eclogite, dry and with H_2O. The effect of fractional crystallization of a basaltic liquid at 100 km depth would probably tend to change liquid compositions further away from the composition join for average basalt–andesite–rhyolite, because the fractionation paths should cross the equilibrium paths from concave to convex sides (Figs. 11, 12, and 14).

Conclusions

We conclude that partial melting of subducted ocean crust with small amounts of H_2O at depths where amphibolite has been converted to quartz eclogite produces liquids of broadly acid or intermediate compositions, but these liquids diverge from the compositions of average calc–alkaline rocks. The products of eclogite fractionation of basaltic liquid would be similar. Therefore, liquids generated from subducted ocean crust at this depth must undergo modifications during uprise which bring them to the calc–alkaline trend. Others have reached similar conclusions from consideration of major- and trace-element contents (Gill, 1974; Lopez-Escobar *et al.*, 1977; Kay, 1977). Nicholls and Ringwood (1973) proposed that siliceous liquids from quartz eclogite could react with overlying peridotite, with subsequent melting of modified mantle producing calc–alkaline andesites. Kay (1977) presented a quantitative treatment of a multistage model to explain the isotope and trace-element chemistry of Aleutian volcanoes. Multistage processes from spreading ridges to subduction zones also have appeal on the grounds of mass balance and isotope data (Armstrong, 1968).

As usual, petrogenetic hypotheses have leapt ahead of quantitative experimental data. The results presented here are not definitive discriminants among the various complex processes currently assumed in subduction zones, despite the urgent need felt for the data in 1971. Nevertheless, the results consolidate information needed where the magmatic processes begin. We need similar results for the total pressure range between the surface and sites of magma generation.

Acknowledgments

This research was supported by the Earth Sciences Section, National Science Foundation, by grants GSA-29426 and EAR 76-20413. It has also been supported in part by the Materials Research Laboratory Program of the National Science Foundation at the University of Chicago. We thank A. T. Anderson and R. C. Newton for their critical reviews of early versions of this material, and P. C. Bateman and F. C. Dodge for the analyzed tonalite.

References

Allen, J. C., A. L. Boettcher and G. Marland (1975) Amphiboles in andesite and basalt: I. Stability as a function of P–T–f_{O_2}. *Am. Mineral., 60,* 1069–1085.

Anderson, A. T. (1974) Chlorine, sulfur, and water in magmas and oceans. *Geol. Soc. Am. Bull., 85,* 1485–1492.

Armstrong, R. L. (1968) A model for the evolution of strontium and lead isotopes in a dynamic earth. *Rev. Geophys., 6,* 175–199.

Boettcher, A. L. (1973) Volcanism and orogenic belts—the origin of andesites. *Tectonophysics, 17,* 223–240.

——— and P. J. Wyllie (1968) Melting of granite with excess water to 30 kilobars pressure. *J. Geol., 76,* 235–244.

Boyd, F. R., P. M. Bell, J. L. England and M. C. Gilbert (1967) Pressure measurement in single-stage apparatus. *Carnegie Inst. Wash. Year Book, 65,* 410–414.

——— and J. L. England (1960) Apparatus for phase-equilibrium measurements at pressures up to 50 kilobars and temperatures up to 1750°C. *J. Geophys. Research, 65,* 741–748.

———, L. W. Finger and F. Chayes (1968) Computer reduction of electron-probe data. *Carnegie Inst. Wash. Year Book, 67,* 210–214.

Carmichael, I. S. E., F. J. Turner and J. Verhoogen (1974) *Igneous Petrology.* McGraw-Hill, New York.

Chayes, F. (1969) The chemical composition of Cenozoic andesites. *Oregon Dept. Geol. Mineral. Industries Bull., 65,* 1–11.

Coats, R. R. (1962) Magma type and crustal structure in the Aleutian arc. *Am. Geophys. Union Monogr., 6,* 92–99.

Dickinson, W. R. (1968) Circum-Pacific andesite types. *J. Geophys. Res., 73,* 2261–2269.

——— (1970) Relations of andesites, granites, and derivative sandstones to arc-trench tectonics. *Rev. Geophys. Space Phys., 8,* 813–860.

——— (1971) Plate tectonic model of geosynclines. *Earth Planet. Sci. Lett., 10,* 165–174.

——— (1973) Widths of modern arc-trench gaps proportional to past duration of igneous activity in associated magmatic arcs. *J. Geophys. Res., 78,* 3376–3389.

——— and T. Hatherton (1967) Andesitic volcanism and seismicity around the Pacific. *Science, 157,* 801–804.

Engel, A. E. J., C. G. Engel and R. G. Havens (1965) Chemical characteristics of oceanic basalts and the upper mantle. *Geol. Soc. Am. Bull., 76,* 719–734.

Getting, I. C. and G. C. Kennedy (1971) The effect of pressure on the E.M.F. of thermocouples. In E. C. Lloyd, Ed., *Accurate Characterization of the High-Pressure Environment,* p. 77–80. U. S. Natl. Bur. Stand., Spec. Pub. 326.

Gill, J. B. (1974) Role of underthrust oceanic crust in the genesis of a Fijian calc–alkaline suite. *Contrib. Mineral. Petrol., 43,* 29–45.

Green, D. H. (1973) Experimental melting studies on a model upper mantle composition at high pressure under water-saturated and water-undersaturated conditions. *Earth Planet. Sci. Lett., 19,* 37–53.

——— (1976) Experimental testing of "equilibrium" partial melting of peridotite under water-saturated, high-pressure conditions. *Can. Mineral., 14,* 255–268.

Green, T. H. (1972) Crystallization of calc–alkaline andesite under controlled high-pressure hydrous conditions. *Contrib. Mineral. Petrol., 34,* 150–166.

——— and A. E. Ringwood (1968) Genesis of the calc–alkaline igneous rock suite. *Contrib. Mineral. Petrol., 18,* 105–162.

——— and ——— (1972) Crystallization of garnet-bearing rhyodacite under high-pressure hydrous conditions. *J. Geol. Soc. Aust., 19,* 203–212.

Hadidiacos, C. G., L. W. Finger and F. R. Boyd (1970) Computer reduction of electron-probe data. *Carnegie Inst. Wash. Year Book, 69,* 294.

Hamilton, W. (1969a) The volcanic central Andes, a modern model for the Cretaceous batholiths and tectonics of western North America. *Oregon Dept. Geol. Mineral. Ind. Bull., 65,* 175–184.

——— (1969b) Mesozoic California and underflow of Pacific mantle. *Bull. Geol. Soc. Am., 80,* 2409–2430.

Jakeš, P. and A. J. R. White (1970) K/Rb ratios of rocks from island arcs. *Geochim. Cosmochim. Acta, 34,* 849–856.

Kay, R. W. (1977) Geochemical constraints on the origin of Aleutian magmas. In M. Talwani and W. C. Pitman III, Eds., *Island Arcs, Deep Sea Trenches and Back-Arc Basins,* p. 229–242. Maurice Ewing Series 1, Am. Geophys. Union, Washington, DC.

Kuno, H. (1960) High-alumina basalt. *J. Petrol., 1,* 121–137.

——— (1966) Lateral variation of basalt magma types across continental margins and island arcs. *Bull. Volcanol., 29,* 195–222.

——— (1968) Origin of andesites and its bearing on the island arc structure. *Bull. Volcanol., 32,* 141–176.

Kushiro, I. (1973) Origin of some magmas in oceanic and circumoceanic regions. *Tectonophysics, 17,* 211–222.

Lambert, I. B. and P. J. Wyllie (1968) Stability of hornblende and a model for the low velocity zone. *Nature, 219,* 1240–1241.

——— and ——— (1972) Melting of gabbro (quartz eclogite) with excess water to 35 kilobars, with geological applications. *J. Geol., 80,* 693–708.

Lopez-Escobar, L., F. A. Frey and M. Vergara (1977) Andesites and high-alumina basalts from the Central-South Chile high Andes: geochemical evidence bearing on their petrogenesis. *Contrib. Mineral. Petrol., 63,* 199–228.

Marsh, D. B. and I. S. E. Carmichael (1974) Benioff zone magmatism. *J. Geophys. Res., 79,* 1196–1206.

Merrill, R. B. and P. J. Wyllie (1973) Iron absorption by platinum capsules in high pressure rock melting experiments. *Am. Mineral., 58,* 16–20.

——— and ——— (1975) Kaersutite and kaersutite eclogite from Kakanui, New Zealand—Water-excess and water-deficient melting at 30 kilobars. *Geol. Soc. Am. Bull., 86,* 55–570.

Muan, A. (1963) Silver–palladium alloys as crucible materials in studies of low-melting iron silicates. *Am. Ceram. Soc. Bull., 42,* 344–347.

Mysen, B. O. and K. S. Heier (1972) Petrogenesis of eclogites in high grade metamorphic gneisses exemplified by the Hareidland eclogite, western Norway. *Contrib. Mineral. Petrol., 36,* 73–94.

Nicholls, I. A. and A. E. Ringwood (1973) Effect of water on olivine stability in tholeiites and the production of silica-saturated magmas in the island-arc environment. *J. Geol., 81,* 285–300.

Nockolds, S. R. (1954) Average chemical compositions of some igneous rocks. *Geol. Soc. Am. Bull., 65,* 1007–1032.

Oxburgh, E. R. and D. L. Turcotte (1970) Thermal structure of island arcs. *Geol. Soc. Am. Bull., 81,* 1665–1688.

Piwinskii, A. J. (1968a) Experimental studies of igneous rock series: Central Sierra Nevada Batholith, California. *J. Geol., 76,* 548–570.

——— (1968b) Studies of batholithic feldspar, Sierra Nevada, California. *Contrib. Mineral. Petrol., 17,* 204–223.

Presnall, D. C. (1969) The geometric analysis of partial fusion. *Am. J. Sci., 267,* 1178–1194.

Raleigh, C. B. and W. H. K. Lee (1969) Sea-floor spreading and island-arc tectonics. *Oreg. Dept. Geol. Mineral. Ind. Bull., 65,* 99–110.

Ringwood, A. E. (1969) Composition and evolution of the upper mantle. In P. J. Hart, Ed., *The Earth's Crust and Upper Mantle,* p. 1–21. Am. Geophys. Monogr. 13.

——— (1975) *Composition and Petrology of the Earth's Mantle.* McGraw-Hill, New York.

Stern, C. R. (1973) *Melting Relations of gabbro–tonalite–granite–red clay with H_2O at 30 kb: the Implications for Melting in Subduction Zones.* Ph.D. Dissertation, University of Chicago.

——— (1974) Melting products of olivine tholeiite basalt in subduction zones. *Geology, 2,* 227–230.

——— and P. J. Wyllie (1973) Melting relations and basalt–andesite–rhyolite–H_2O and a pelagic red clay at 30 kilobars. *Contrib. Mineral. Petrol., 42,* 313–323.

——— and ——— (1975) Effect of iron absorption by noble-metal capsules on phase boundaries in rock-melting experiments at 30 kilobars. *Am. Mineral., 60,* 681–689.

———, W-L. Huang and P. J. Wyllie (1975) Basalt–andesite–rhyolite–H_2O: crystallization intervals with excess H_2O and H_2O-undersaturated liquidus surfaces to 35 kilobars, with implications for magma genesis. *Earth Planet. Sci. Lett., 26,* 189–196.

Stille, H. (1955) Recent deformation of the earth's crust in the light of those of earlier epochs. *Geol. Soc. Am. Spec. Pap., 62,* 172–192.

Sugimura, A. (1968) Spatial relations of basaltic magmas in island arcs. In H. H. Hess and A. Poldervaart, Eds., *Basalts,* v.2, 573–601. Interscience, New York.

Taylor, S. R. and A. J. R. White (1966) Trace element abundance in andesites. *Bull. Volcanol., 29,* 177–194.

Van der Plas, L. and A. Tobi (1965) A chart for judging the reliability of point count results. *Am. J. Sci., 263,* 67–90.

Wise, W. S. (1969) Geology and petrology of the Mount Hood area: a study of High Cascade volcanism. *Geol. Soc. Am. Bull., 80,* 969–1006.

Wyllie, P. J. (1971) *The Dynamic Earth: Textbook in Geosciences.* Wiley, New York.

——— (1973) Experimental petrology and global tectonics—a preview. *Tectonophysics, 17,* 189–209.

——— (1977) From crucibles through subduction to batholiths. In S. K. Saxena and S. Bhattacharji, Eds., *Energetics of Geological Processes,* p. 389–433. Springer-Verlag, New York.

——— and H. I. Drever (1963) The petrology of picritic rocks, a picrite sill in the Island of Soay (Hebrides). *R. Soc. Edinburgh Trans., 65,* 155–177.

Yoder, H. S. and C. E. Tilley (1962) Origin of basalt magmas: an experimental study of natural and synthetic rock systems. *J. Petrol., 3,* 342–532.

Manuscript received, November 14, 1977; accepted for publication, March 23, 1978.